TABLE 1. Specific activities of mitochondrial respiratory enzymes in *E. multilocularis* protoscoleces

Assay	Sp act[a] (nmol/min/mg of protein) (mean ± SD)
SDH	103 ± 16
Succinate-quinone reductase	
dUQ (anaerobic)	98.9 ± 12
dRQ (anaerobic)	16.6 ± 3.5
Quinol-fumarate reductase (decyl rhodoquinol) (anaerobic)	60.2 ± 18
NADH oxidase	9.1 ± 2.1
NADH oxidase with:	
2 mM KCN	7.3 ± 1.5
100 mM malonate	4.4 ± 0.4
2 mM KCN and 100 mM malonate	1.7 ± 0.7
Ubiquinol-1 oxidase	4.4 ± 0.6
TMPD oxidase	12.6 ± 6.3
NADH-fumarate reductase (anaerobic)	45.0 ± 8.1
NADH-quinone reductase	
dUQ (anaerobic)	32.1 ± 2.7
dRQ (anaerobic)	61.3 ± 4.3

[a] Specific activities were obtained from at least three independently isolated mitochondria.

min/mg, respectively. These activities were completely inhibited by 2 mM KCN. Under anaerobic conditions, the specific activity of NADH-fumarate reductase was 45 nmol/min/mg, which was much higher than the NADH oxidase activity. The specific activity of NADH-dUQ reductase and NADH-dRQ reductase of complex I were determined to be 32.1 and 61.3 nmol/min/mg, respectively.

Quinone components in *E. multilocularis* mitochondria. To determine which quinones act as physiological electron mediators in the mitochondrial respiratory system of *E. multilocularis* protoscoleces, HPLC analyses were performed. As shown in Fig. 4A, the enriched mitochondrial fractions contained only one major quinone component at a retention time (*Rt*) of 22.4 min. The peak fraction exhibited a characteristic absorption maximum for RQs at 283 nm (Fig. 4B) (20). Subsequent MS analysis confirmed that the primary quinone of the parasite was RQ_{10} (electrospray ionization-MS *m/z* 848.8 $[M + H]^+$). The concentration of RQ_{10} was determined to be 0.73 nmol/mg of mitochondrial protein.

Effects of inhibitors on NADH-fumarate reductase in *E. multilocularis* mitochondria. To investigate the inhibitory effect of quinazoline (Fig. 5A) and its derivatives on the enzymatic activities in the anaerobic respiratory system of *E. multilocularis* mitochondria, we determined IC_{50} values against the NADH-fumarate reductase activity of the enriched mitochondrial fraction of the parasite. We found that all of the compounds inhibited the NADH-fumarate reductase activity of the parasite to some extent. Quinazoline and its derivatives including 6-NH_2, 6-NHCO($CH{=}CH_2$), 7-NH_2, 8-OH, 8-OCH_3, 8-OCH_2CH_3, and 8-$OCH(CH_3)_2$ exhibited IC_{50} values of 2.3, 2.1, 16, 62, 71, 48, 4,100, and 910 nM, respectively. Of the compounds tested, the 8-OH derivative (Fig. 5B) exhibited relatively selective inhibition against the NADH-fumarate reductase activity of *E. multilocularis* protoscoleces compared with the NADH oxidase activities of mammalian mitochondria: the IC_{50} values of quinazoline and its 8-OH derivative for

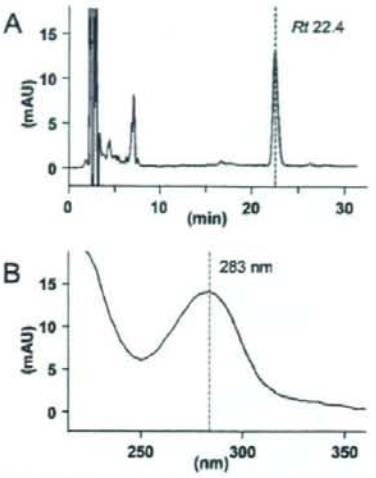

FIG. 4. (A) HPLC analysis of quinones extracted from the enriched mitochondrial fraction of *E. multilocularis* protoscoleces. Detailed experimental conditions are described in Materials and Methods. The highest peak had a retention time of 22.4 min (arrow). (B) Absorption of this peak was 283 nm, suggesting that it contained an RQ. mAU, milli-absorbance units.

the NADH oxidase activities of mammalian (bovine heart) mitochondria were 0.40 and 230 nM, respectively.

Effects of inhibitors on living *E. multilocularis* protoscoleces. In order to examine the parasite-killing activities of the quinazoline-type compounds with different degrees of inhibitory effects against NADH-fumarate activities of *E. multilocularis* protoscoleces, we performed in vitro treatment of the parasite using quinazoline and its 8-OH derivative. The viability of the *E. multilocularis* protoscolex was progressively reduced during in vitro treatment of the parasites with 50 μM of the 8-OH derivative, and by day 5, all the parasites died (Fig. 6). The same compound did not have an obvious antiparasitic effect when used at a concentration of 5 μM. On the other hand, nonsubstituted quinazoline, which showed lower IC_{50} values with the enzymatic assay, eliminated the parasites on days 5 and 7 of in vitro treatment when used at 50 and 5 μM, respectively. Treatment with rotenone, a specific inhibitor of mitochondrial complex I (19), affected the viability of the parasite in a manner similar to that of the 8-OH derivative. The anti-echinococcal effect of nitazoxanide was relatively mild: even in

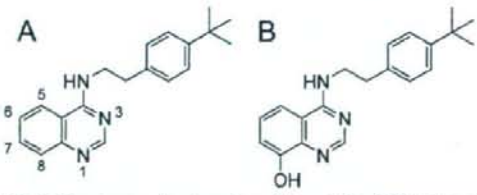

FIG. 5. Structures of quinazoline (A) and its 8-OH derivative (B) used for the enzyme inhibition assays and in vitro treatment of *E. multilocularis* protoscoleces.

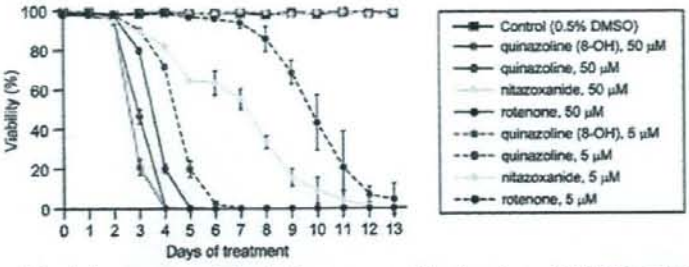

FIG. 6. Viability of *E. multilocularis* protoscoleces during in vitro treatment with quinazoline and its 8-OH derivatives, rotenone and nitazoxanide. Each compound was added to the culture medium at 5 or 50 μM. The results represent the means ± standard deviations of at least triplicate samples. DMSO, dimethyl sulfoxide.

the presence of 50 μM nitazoxanide, the viability decreased, but it did so only gradually, and it took 13 days before all the protoscoleces died. This compound did not affect parasite viability when used at 5 μM.

DISCUSSION

The most notable finding of the present study is that *E. multilocularis* protoscoleces possess a unique mitochondrial respiratory system that is highly adapted to anaerobic conditions. Specifically, the predominant enzymatic activity in the enriched mitochondrial fraction prepared from the parasite protoscoleces is the NADH-fumarate reductase system, which does not normally function in the aerobic respiratory chain of mammals. Thus, we infer that mitochondrial respiratory system of *E. multilocularis* would be a good target for the development of novel selective antiechinococcal compounds as demonstrated previously for other helminthic diseases (8, 21).

As early as 1957, Agosin found that *E. granulosus* protoscoleces have both aerobic and anaerobic respiratory systems and that glycolytic inhibitors are effective against both of them, indicating that they both depend on glycolysis (1). Subsequently, McManus and Smyth observed that protoscoleces cultured under anaerobic conditions produce more succinate than parasites kept under aerobic conditions, suggesting that the parasites survive under anaerobic conditions by utilizing the NADH-fumarate reductase system (16). Furthermore, McManus and Smyth reported that the specific activity of fumarate reductase in *Echinococcus* protoscoleces is lower than those of enzymes involved in the tricarboxylic acid cycle (17). These results, however, did not establish the importance of NADH-fumarate reductase activity in the mitochondrial respiratory system of the parasite because the other enzyme activities were not analyzed.

In the present study, we focused on the enzyme activities of the mitochondrial respiratory system of the parasite to determine whether the system is adapted to anaerobic conditions. Using the enriched mitochondrial fractions prepared from *E. multilocularis* protoscoleces, we showed that the activity of NADH-fumarate reductase in the respiratory system of the parasite is predominant compared with that of NADH oxidase, an enzyme involved in aerobic respiration in aerobic organisms such as mammals. Furthermore, direct measurements of complex II activities in both directions (i.e., succinate-RQ reductase and rhodoquinol-fumarate reductase activities) indicated that parasite complex II functions more favorably as a rhodoquinol-fumarate reductase in the presence of RQ/rhodoquinol. Thus, our results using isolated mitochondria of *E. multilocularis* protoscoleces coupled with assay systems for the determination of the parasite's enzyme activities revealed for the first time that the parasite mitochondria are highly adapted to anaerobic environments.

Analyses of the quinone components of *E. multilocularis* mitochondria revealed that RQ_{10} (Fig. 1B), whose redox potential is much more negative (E_m' [midpoint potential] = −63 mV) than that of UQ_{10} (E_m' = +110 mV) (Fig. 1A), was the primary quinone component of parasite mitochondria. In other parasitic helminths, like *A. suum* and *Hymenolepis diminuta*, RQ is an essential component of the NADH-fumarate reductase system (5, 11). In addition, van Hellemond et al. previously demonstrated that for all eukaryotes, the relative amount of RQ compared to the total amount of quinones correlates well with the importance of fumarate reduction in vivo (31). Similarly, during the development of the liver fluke *Fasciola hepatica*, there is a good correlation between the quinone composition and the importance of fumarate reduction in vivo (31). Therefore, RQ seems to be an essential component of fumarate reduction in eukaryotic respiration. Although menaquinone-related fumarate reduction in prokaryotes is well known (33, 34), there is no evidence that menaquinone serves this function in eukaryotes. In this study, enzyme assays demonstrated that the mitochondria from *E. multilocularis* possess NADH-fumarate activity as the predominant activity. In addition, the NADH-dRQ reductase activity was much higher than that of NADH-dUQ reductase, indicating that *E. multilocularis* complex I may interact preferentially with RQ rather than with UQ. Taken together, these results indicate that, as in other metazoan eukaryotes with anaerobic respiratory systems, *E. multilocularis* protoscoleces have a unique respiratory system that is highly adapted to anaerobic environments and in which RQ_{10} is used as the primary electron mediator.

Spiliotis et al. recently reported that the in vitro growth of larval *E. multilocularis* is more active under anaerobic than aerobic conditions (23). Thus, our findings for the respiratory system of *E. multilocularis* protoscoleces are consistent with the observations reported previously by Spiliotis et al. Larval *E. multilocularis* containing a large number of protoscoleces

lives in host tissues, mainly the liver, surrounded by thick connective tissues containing carbohydrate-rich laminated layers, which probably provide the parasite cells with an extremely-low-oxygen environment. Accordingly, it is not surprising that the parasite survives in the host by utilizing an anaerobic respiratory system.

Many anaerobic parasitic eukaryotes use the NADH-fumarate pathway, which is absent in mammals (2, 3, 10, 14, 22, 29). Therefore, this unique respiratory system is regarded as a promising chemotherapeutic target for the development of novel anthelminthics, as discussed in a recent review (9). In fact, Omura et al. previously found a natural compound, nafuredin, that is a potent inhibitor of the adult *A. suum* mitochondrial respiratory chain but much weaker against the mammalian mitochondrial respiratory chain (21). Yamashita et al. also found that quinazoline-type inhibitors were highly effective against adult *A. suum* complex I (35). Kinetic analyses using a series of quinazoline-type inhibitors revealed that *A. suum* complex I recognizes RQ_2 or UQ_2 in different ways, suggesting that mitochondrial complex I, which reacts preferably with RQs, could be a good target for chemotherapy. In the present study, we also tested several quinazoline-type compounds for their abilities to inhibit the anaerobic respiratory system of *E. multilocularis* protoscoleces. We found that all of the quinazoline-type compounds inhibited the NADH-fumarate reductase activity of *E. multilocularis* mitochondria to different extents. Furthermore, these compounds exhibited potent parasite-killing activities against *E. multilocularis* protoscoleces under in vitro culture conditions. Importantly, the nonsubstituted quinazoline, which has a higher inhibitory effect against NADH-fumarate oxidoreductase of the parasite mitochondria than the 8-OH derivative does, exhibited the parasite-killing activity even when used at 5 μM, whereas the 8-OH derivative did not do so at the same concentration. Such a correlation between the enzyme inhibition and the parasite-killing activities of these compounds suggests that the anaerobic NADH-fumarate reductase system of the parasite is a promising target for the development of antiechinococcal drugs.

Antiechinococcal drugs for chemotherapy of human AE should target not only protoscoleces but also the germinal layers of the *E. multilocularis* metacestode. The germinal layers in the larval parasite exhibit extremely unique characteristics. The parasite cells forming the germinal layers can differentiate into various tissues, including brood capsules and protoscoleces, and at the same time, they proliferate asexually as they remain in an undifferentiated state. This causes enlargement and, occasionally, metastasis of the lesions due to the formation of a large parasite mass. Therefore, for chemotherapy of AE, a complete cure cannot be achieved unless the germinal cells of the larval parasite are eliminated. Therefore, the mitochondrial respiratory system of germinal cells should be further characterized to aid in the development of a novel antiechinococcal compound(s) targeting the energy metabolism of larval *E. multilocularis*. However, it is presently quite difficult to obtain enough metacetode materials with homogeneous quality. Established methodologies for the in vitro cultivation of *E. multilocularis* metacestodes are now available (6, 23), and they will hopefully be applicable to large-scale preparations of metacestode materials in the near future.

During the life cycle of *E. multilocularis*, the parasite never undergoes active development and/or energy metabolism under aerobic conditions. The larval parasite lives mainly in the liver of intermediate host animals, whereas the adult worm dwells inside the small intestine of the final host, both of which are microaerobic conditions. Although the eggs of the parasite are exposed to air, they already contain a mature infective larva (oncosphere) waiting to be taken up by the next intermediate host. Therefore, the oncosphere does not develop or move under aerobic conditions. Taken together, these findings suggest that the respiratory system of *E. multilocularis* protoscoleces, as characterized in the present study, could represent the respiratory system used by the parasite throughout its developmental stages. Based on this speculation, the use of protoscolex materials in the first-step screening of candidate compounds by enzyme inhibition assays and subsequent in vitro parasite-killing assays appears to be reasonable, although it should be confirmed that the respiratory system of the *E. multilocularis* metacestode shares the same basic characteristics with that of the protoscolex stage of the parasite. We have already done preliminary experiments on the effects of the compounds used in this study, including the quinazoline derivative (8-OH), against in vitro-cultured metacestodes and found that the compounds exhibited high parasite-killing activities as evaluated by a modified MTT assay (data not shown). These results strongly suggest that our strategy is appropriate.

Highly effective chemotherapeutic compounds against human AE are not currently available despite the fact that the disease can be lethal unless the patient is appropriately treated during the early stage of the infection. Based on the findings presented here, it appears that the anaerobic respiratory system of *E. multilocularis*, which is distinct from that of host mammals, is a good target for the development of highly effective antiechinococcal drugs and, furthermore, that respiratory chain inhibitors (21, 35) are possible lead compounds for the development of antiechinococcal drugs.

ACKNOWLEDGMENTS

We thank Andrew Hemphill at the University of Berne for kindly providing us with precious chemical compounds.

This work was supported by grants from the following organizations: the Ministry of Education, Culture, Sports, Science, and Technology of Japan for the 21st Century COE Program, Program of Excellence for Zoonosis Control, and 18073004; the Ministry of Health and Welfare, Japan, for the Control of Emerging and Reemerging Diseases in Japan; the Japan Society of the Promotion of Science (grants 17790274 and 18GS0314); the Northern Advancement Center for Science and Technology; and the Akiyama Foundation.

REFERENCES

1. **Agosin, M.** 1957. Studies on the metabolism of *Echinococcus granulosus*. II. Some observations on the carbohydrate metabolism of hydatid cyst scolices. Exp. Parasitol. 6:586–593.
2. **Amino, H., A. Osanai, H. Miyadera, N. Shinjyo, T. Tomitsuka, H. Taka, R. Mineki, K. Murayama, S. Takamiya, T. Aoki, H. Miyoshi, K. Sakamoto, S. Kojima, and K. Kita.** 2003. Isolation and characterization of the stage-specific cytochrome *b* small subunit (CybS) of *Ascaris suum* complex II from the aerobic respiratory chain of larval mitochondria. Mol. Biochem. Parasitol. **128**:175–186.
3. **Amino, H., H. Wang, H. Hirawake, F. Saruta, D. Mizuchi, R. Mineki, N. Shindo, K. Murayama, S. Takamiya, T. Aoki, S. Kojima, and K. Kita.** 2000. Stage-specific isoforms of *Ascaris suum* complex. II. The fumarate reductase of the parasitic adult and the succinate dehydrogenase of free-living larvae share a common iron-sulfur subunit. Mol. Biochem. Parasitol. **106**:63–76.
4. **Bryant, C., and C. Behm.** 1989. Energy metabolism, p. 25–69. *In* C. Bryant

and C. Behm (ed.), Biochemical adaptation in parasites. Chapman and Hall, London, United Kingdom.
5. **Fioravanti, C. F., and Y. Kim.** 1988. Rhodoquinone requirement of the *Hymenolepis diminuta* mitochondrial electron transport system. Mol. Biochem. Parasitol. **28:**129–134.
6. **Hemphill, A., and B. Gottstein.** 1995. Immunology and morphology studies on the proliferation of in vitro cultivated *Echinococcus multilocularis* metacestodes. Parasitol. Res. **81:**605–614.
7. **Kita, K., H. Hirawake, and S. Takamiya.** 1997. Cytochromes in the respiratory chain of helminth mitochondria. Int. J. Parasitol. **27:**617–630.
8. **Kita, K., C. Nihei, and E. Tomitsuka.** 2003. Parasite mitochondria as drug target: diversity and dynamic changes during the life cycle. Curr. Med. Chem. **10:**2535–2548.
9. **Kita, K., K. Shiomi, and S. Omura.** 2007. Advances in drug discovery and biochemical studies. Trends Parasitol. **23:**223–229.
10. **Kita, K., and S. Takamiya.** 2002. Electron-transfer complexes in *Ascaris* mitochondria. Adv. Parasitol. **51:**95–131.
11. **Kita, K., S. Takamiya, R. Furushima, Y. Ma, H. Suzuki, T. Ozawa, and H. Oya.** 1988. Electron-transfer complexes of *Ascaris suum* muscle mitochondria. III. Composition and fumarate reductase activity of complex II. Biochim. Biophys. Acta **935:**130–140.
12. **Köhler, P.** 1991. The pathways of energy generation in filarial parasites. Parasitol. Today **7:**21–25.
13. **Komuniecki, R., and B. G. Harris.** 1995. Carbohydrate and energy metabolism in helminths, p. 49–66. *In* J. J. Marr and M. Müller (ed.), Biochemistry and molecular biology of parasites. Academic Press, New York, NY.
14. **Kuramochi, T., H. Hirawake, S. Kojima, S. Takamiya, R. Furushima, T. Aoki, R. Komuniecki, and K. Kita.** 1994. Sequence comparison between the flavoprotein subunit of the fumarate reductase (complex II) of the anaerobic parasitic nematode, *Ascaris suum* and the succinate dehydrogenase of the aerobic, free-living nematode, *Caenorhabditis elegans*. Mol. Biochem. Parasitol. **68:**177–187.
15. **Lowry, O. H., N. J. Rosebrough, A. L. Farr, and R. J. Randall.** 1951. Protein measurement with the Folin phenol reagent. J. Biol. Chem. **193:**265–275.
16. **McManus, D. P., and J. D. Smyth.** 1978. Differences in the chemical composition and carbohydrate metabolism of *Echinococcus granulosus* (horse and sheep strains) and *E. multilocularis*. Parasitology **77:**103–109.
17. **McManus, D. P., and J. D. Smyth.** 1982. Intermediary carbohydrate metabolism in protoscoleces of *Echinococcus granulosus* (horse and sheep strains) and *E. multilocularis*. Parasitology **84:**351–366.
18. **McManus, D. P., W. Zhang, J. Li, and P. B. Bartley.** 2003. Echinococcosis. Lancet **362:**1295–1304.
19. **Miyoshi, H.** 1998. Structure-activity relationships of some complex I inhibitors. Biochim. Biophys. Acta **1364:**236–244.
20. **Moore, H. W., and K. Folkers.** 1965. Coenzyme Q. LXII. Structure and synthesis of rhodoquinone, a natural aminoquinone of the coenzyme Q group. J. Am. Chem. Soc. **87:**1409–1410.
21. **Omura, S., H. Miyadera, H. Ui, K. Shiomi, Y. Yamaguchi, R. Masuma, T. Nagamitsu, D. Takano, T. Sunazuka, A. Harder, H. Kölbl, M. Namikoshi, H. Miyoshi, K. Sakamoto, and K. Kita.** 2001. An anthelmintic compound, nafuredin, shows selective inhibition of complex I in helminth mitochondria. Proc. Natl. Acad. Sci. USA **98:**60–62.
22. **Saruta, F., T. Kuramochi, K. Nakamura, S. Takamiya, Y. Yu, T. Aoki, K. Sekimizu, S. Kojima, and K. Kita.** 1995. Stage-specific isoforms of complex II (succinate-ubiquinone oxidoreductase) in mitochondria from the parasitic nematode, *Ascaris suum*. J. Biol. Chem. **270:**928–932.
23. **Spiliotis, M., D. Tappe, L. Sesterhenn, and K. Brehm.** 2004. Long-term in vitro cultivation of *Echinococcus multilocularis* metacestodes under axenic conditions. Parasitol. Res. **92:**430–432.
24. **Takada, M., S. Ikenoya, T. Yuzuriha, and K. Katayama.** 1982. Studies on reduced and oxidized coenzyme Q (ubiquinones). II. The determination of oxidation-reduction levels of coenzyme Q in mitochondria, microsomes and plasma by high-performance liquid chromatography. Biochim. Biophys. Acta **679:**308–314.
25. **Takamiya, S., R. Furushima, and H. Oya.** 1984. Electron transfer complexes of *Ascaris suum* muscle mitochondria. I. Characterization of NADH-cytochrome *c* reductase (complex I-III), with special reference to cytochrome localization. Mol. Biochem. Parasitol. **13:**121–134.
26. **Takamiya, S., K. Kita, H. Wang, P. P. Weinstein, A. Hiraishi, H. Oya, and T. Aoki.** 1993. Developmental changes in the respiratory chain of *Ascaris* mitochondria. Biochim. Biophys. Acta **1141:**65–74.
27. **Thompson, R. C., P. Deplazes, and J. Eckert.** 1990. Uniform strobilar development of *Echinococcus multilocularis* in vitro from protoscolex to immature stages. J. Parasitol. **76:**240–247.
28. **Tielens, A. G. M., C. Rotte, J. J. van Hellemond, and W. Martin.** 2002. Mitochondria as we don't know them. Trends Biochem. Sci. **27:**564–572.
29. **Tielens, A. G. M., and J. J. van Hellemond.** 1998. The electron transport chain in anaerobically functioning eukaryotes. Biochim. Biophys. Acta **1365:** 71–78.
30. **Towbin, H., T. Staehelin, and J. Gordon.** 1979. Electrophoretic transfer of proteins from polyacrylamide gels to nitrocellulose sheets: procedure and some applications. Proc. Natl. Acad. Sci. USA **76:**4350–4354.
31. **van Hellemond, J. J., M. Klockiewicz, C. P. Gaasenbeek, M. H. Roos, and A. G. M. Tielens.** 1995. Rhodoquinone and complex II of the electron transport chain in anaerobically functioning eukaryotes. J. Biol. Chem. **270:** 31065–31070.
32. **Walker, M., J. F. Rossignol, P. Torgerson, and A. Hemphill.** 2004. In vitro effects of nitazoxanide on *Echinococcus granulosus* protoscoleces and metacestodes. J. Antimicrob. Chemother. **54:**609–616.
33. **Wissenbach, U., A. Kroger, and G. Unden.** 1990. The specific functions of menaquinone and demethylmenaquinone in anaerobic respiration with fumarate, dimethylsulfoxide, trimethylamine *N*-oxide and nitrate by *Escherichia coli*. Arch. Microbiol. **154:**60–66.
34. **Wissenbach, U., D. Ternes, and G. Unden.** 1992. An *Escherichia coli* mutant containing only demethylmenaquinone, but no menaquinone: effects on fumarate, dimethylsulfoxide, trimethylamine *N*-oxide and nitrate respiration. Arch. Microbiol. **158:**68–73.
35. **Yamashita, T., T. Ino, H. Miyoshi, K. Sakamoto, A. Osanai, E. Nakamaru-Ogiso, and K. Kita.** 2004. Rhodoquinone reaction site of mitochondrial complex I, in parasitic helminth, *Ascaris suum*. Biochim. Biophys. Acta **1608:** 97–103.

Available online at www.sciencedirect.com
ScienceDirect
Parasitology International 57 (2008) 229–232
www.elsevier.com/locate/parint

Short communication

Mutation underlying resistance of *Plasmodium berghei* to atovaquone in the quinone binding domain 2 (Qo_2) of the cytochrome *b* gene

Josephine E. Siregar [a,d], Din Syafruddin [a,b], Hiroyuki Matsuoka [c], Kiyoshi Kita [d], Sangkot Marzuki [a,*]

[a] *Eijkman Institute for Molecular Biology, Jakarta, Indonesia*
[b] *Department of Parasitology, Faculty of Medicine, Hasanuddin University, Makassar, Indonesia*
[c] *Department of Medical Zoology, Jichi Medical University, Tochigi, Japan*
[d] *Department of Biomedical Chemistry, Graduate School of Medicine, The University of Tokyo, Tokyo, Japan*

Received 7 March 2007; received in revised form 29 November 2007; accepted 1 December 2007
Available online 8 December 2007

Abstract

The anti-malarial agent atovaquone specifically targets the cytochrome bc_1 complex and inhibits the parasite respiration. Resistance to this drug, a coenzyme Q analogue, is associated with mutations in the mitochondrial cytochrome *b* gene. We previously reported atovaquone resistant mutations in *Plasmodium berghei*, in the first quinone binding domain (Qo_1) of the cytochrome *b* gene (M133I and L144S) with V284F in the sixth transmembrane domain. However, in *P. falciparum* the most common mutations are found in the Qo_2 region. To obtain a better model for biochemical and genetic studies, we have now extended our study to isolate a wider range of *P. berghei* resistant strains, in particular those in the Qo_2. Here we report four new mutations (Y268N, Y268C, L271V and K272R), all in the Qo_2 domain. Two of these mutations are convergent to codon 268 (nt802–804) drug-induced mutation in *P. falciparum*.

Keywords: *Plasmodium berghei*; Cytochrome *b* gene mutations; Atovaquone resistance

The emergence of drug-resistant strains of *Plasmodium falciparum* within the last few decades has caused major problems in malaria treatment and control in many endemic countries. New affordable drugs that target different biochemical pathways in the malaria parasite are needed. Atovaquone, a hydroxy-1,4,-naphthoquinone, is an anti-malaria that shares structural similarity with protozoan ubiquinone, a coenzyme involved in the mitochondrial electron transport [1,2]. It is effective against chloroquine-resistant strains of *P. falciparum*, and is a major component of Malarone™ (a fixed combination of atovaquone and proguanil).

This drug collapses mitochondrial membrane potential in *Plasmodium* spp [3], and is suggested to act by competitive binding with ubiquinone at the quinone binding domain of the quinol-cytochrome *c* reductase of the mitochondrial respiratory chain (bc_1 complex, also referred to as complex III). Mutations conferring atovaquone resistance were identified in the mitochondrial cytochrome *b* (*cytb*) gene of *P. berghei* [4], *P. yoelii* [5], *P. falciparum* [6], *Pneumocystis carinii* [7], and *Toxoplasma gondii* [8]. In *Plasmodium* spp, 10 mutations, M133I, L144S, I258M, F267I, Y268C/N/S, L271F/V, K272R, P275T, G280D, and V284F had been documented, mostly located in the quinone binding domain 2 (Qo_2). Significantly, mutations affecting codon 268 (nt802–804) of the *cytb* gene in the Qo_2 domain, have been reported also in *P. falciparum* isolates collected from malaria-infected individuals in Africa, associated with the use of, and in some cases with demonstrated treatment-failure against Malarone [9–11], leading to the suggestion for its use as a molecular marker for atovaquone resistance in the field isolates [12].

The two main *P. berghei* mutations reported previously [4], M133I and L144S, were all located in the quinone binding domain 1 (Qo_1); these mutations confer up to 1000-fold

* Corresponding author. Eijkman Institute for Molecular Biology, Jalan Diponegoro 69, Jakarta 10430, Indonesia. Tel.: +62 21 3917131; fax: +62 21 3147982.
E-mail address: smarzuki@eijkman.go.id (S. Marzuki).

1383-5769/$ - see front matter © 2007 Elsevier Ireland Ltd. All rights reserved.
doi:10.1016/j.parint.2007.12.002

resistance in combination with V284F in the sixth transmembrane domain, which is adjacent to Qo_2 site. To obtain a better model for the biochemical and genetic studies of mutations observed in the human *P. falciparum*, we have now extended our study to isolate a wider range of *P. berghei* resistant strains, in particular those in the Qo_2 region conferring high degrees of resistance. Here we report four new mutations, most in the Qo_2 domain, two of which are convergent to codon 268 mutations in *P. falciparum*.

P. berghei ANKA strains were inoculated intraperitoneally into 10–12 week old BALB/c mice at approx 10^7 parasitized red blood cells/mouse. At the parasitemia level of 1–5%, the *P. berghei*-infected mice were treated intraperitoneally with different doses of atovaquone, between 0.5 and 14.4 mg kg^{-1} BW as specified in Table 1, daily for three consecutive days. Parasites were then allowed to recover for 7 days in the absence of the drug, before the same daily treatment was introduced for another 3 days. This cycle of treatment was repeated until resistance was observed, as indicated by level of parasitemia which was monitored daily. The resistant parasites were then reinoculated intraperitoneally into 10–12 week old BALB/c mice to obtain enough parasites for drug resistance test (legend of Table 1) and cryofreezing. Some isolates were further cloned by serial limiting dilution and reisolation in mice. Ten isolates were obtained, PbLSJ1 to 8 derived from *P. berghei* ANKA Leiden, and PbESJ9 and 10 from *P. berghei* ANKA Edinburgh (Table 1). In addition PbSK2A1Tb was obtained by following two passages of a frozen PbSK2A1T resistant line from our previous study [4].

Table 1
Atovaquone-resistant isolates of *P. berghei*

Isolates[a]	Atovaquone challenge[b] (mg kg^{-1} BW)	Mutation	ED50[c] (mg kg^{-1} BW)	Growth rate[d] (correlation coefficient)
PbLSJ1.1	14.4	Y268N	80	0.61 (0.96)
PbLSJ2.1	14.4	Y268C	5.2	0.86 (0.84)
PbLSJ3.1	14.4	L271V+ K272R	16	1.48 (0.96)
PbESJ9	14.4	L271V+ K272R	N.D	N.D
PbESJ10	14.4	L271V+ K272R	N.D	N.D
PbSK2A1Tb	Previous study [4]	M133I+ L271V	4	1.64 (0.84)
PbLSJ6	8	Y268N	N.D	N.D
PbLSJ4	4	Y268N	N.D	N.D
PbLSJ7	4	Y268C	N.D	N.D
PbLSJ5	2	L271V+ K272R	N.D	N.D
PbLSJ8	1	L271V+ K272R	N.D	N.D
PbL	Control	Wild type	0.01	6.05 (0.93)

[a] PbLSJ1-8 refer to mutants derived from *P. berghei* ANKA Leiden, while PbESJ9-10 from *P. berghei* ANKA Edinburgh. PbSK2A1Tb appeared following two passages of a frozen PbSK2A1T resistant strain isolated in our previous study [4]; Repeated sequencing confirmed the presence of M133I and V284F in the frozen original PbSK2A1T.

[b] The concentrations of atovaquone indicated are those employed in the isolation of resistant mutants, by treating *P. berghei*-infected BALB/c mice in cycles of 3 days of treatment and 7 days of recovery as described in the text.

[c] Drug resistance test was carried out by inoculating parasite isolates intraperitoneally into the 10–12 week old BALB/c mice, and challenging the infected mice with atovaquone at daily doses ranging from 0.001 to 50 mg kg^{-1} BW. Between three and four mice were used per *P. berghei* isolate per dose of atovaquone. Growth of parasites was determined by daily monitoring of parasitemia for 4–6 days. The 50% Effective Dose (ED50) and correlation coefficient values were calculated from the growth rates of each *P. berghei* isolate during the daily treatment with atovaquone, employing the Sigmoidal Regression Wizard.

[d] Growth rate is expressed as % increase in parasitemia day^{-1}.

A region of the 6 kb mitochondrial DNA (mtDNA) of the various *P. berghei* isolates (nt3368–nt5019) was amplified and sequenced. This region spanned the entire *cytb* gene and, therefore, includes the Qo_1 and Qo_2 domains associated with atovaquone resistance mutations [4,5]. A T to A nucleotide substitution at the first base of codon 268 (nt802) was found in three isolates (PbLSJ1.1, PbLSJ4 and PbLSJ6), leading to amino acid change Y268N in the Qo_2 domain (Table 1). Two other isolates carried an A to G substitution at the second base of the same codon (nt803), leading to amino acid change Y268C (PbLSJ2.1 and PbLSJ7). The remaining five isolates were all double mutants, carrying a T to G nucleotide substitution at nt811 and an A to G at nt815, leading to L271V and K272R, respectively. PbSK2A1Tb carried the Qo_1 G to A substitution at nt399, leading to M133I, as observed in its parental PbSK2A1T line [4], and the T to G substitution at nt811 leading to L271V in the Qo_2 domain were confirmed. Interestingly, the transmembrane V284F amino acid change of the parental line PbSK2A1T [4] has apparently disappeared during the two passages in mice.

The level of resistance of four representative isolates was determined *in vivo* as described in Table 1. The ED_{50} for the parental *P. berghei* ANKA line was found to be 0.01 mg atovaquone kg^{-1} BW, PbSJ1.1 (Y268N) showed the highest degree of resistance, with an ED_{50} of 80 mg kg^{-1} BW, while those for PbSJ2 (Y268C) and PbSJ3 (L271V+K272R) were 5.2 and 16 mg kg^{-1} BW, respectively. PbSK2A1Tb that had both Qo_1 and Qo_2 mutations (M133I+L271V) showed similar order of resistance, with an ED_{50} of 4 mg kg^{-1} BW (Table 1).

All of the mutations found in the present study are located in Qo_2 (Fig. 1), the ubiquinol oxidation domain of the cytochrome *b*, where the electron transfer to the iron–sulphur protein, and the consequent charge separation, results in proton translocation. This is in contrast to results of our earlier attempt to isolate atovaquone resistance mutants of *P. berghei* [4], which had lead to mutations in the Qo_1 domain. In the earlier study mutants were isolated by the exposure of the *P. berghei in vivo* to increasing doses of atovaquone, whereas in the present study the parasite was challenged with repeated cycles of exposure and recovery of single doses of the anti-malaria drug. It is possible that the former procedure has allowed the development of perhaps weaker Qo_1 mutants. The latter is closer to the situation in clinical treatment of malaria, and it is thus of interest to observe similar Qo_2 mutations in field isolates of *P. falciparum*(Y268S, Y268N and Y268C) [6,9,11]. Further, the isolation of *P. falciparum* resistant strains *in vitro*, by the exposure of cultured parasites with step-wise increasing doses of atovaquone, resulted in combinations of Qo_1 and Qo_2

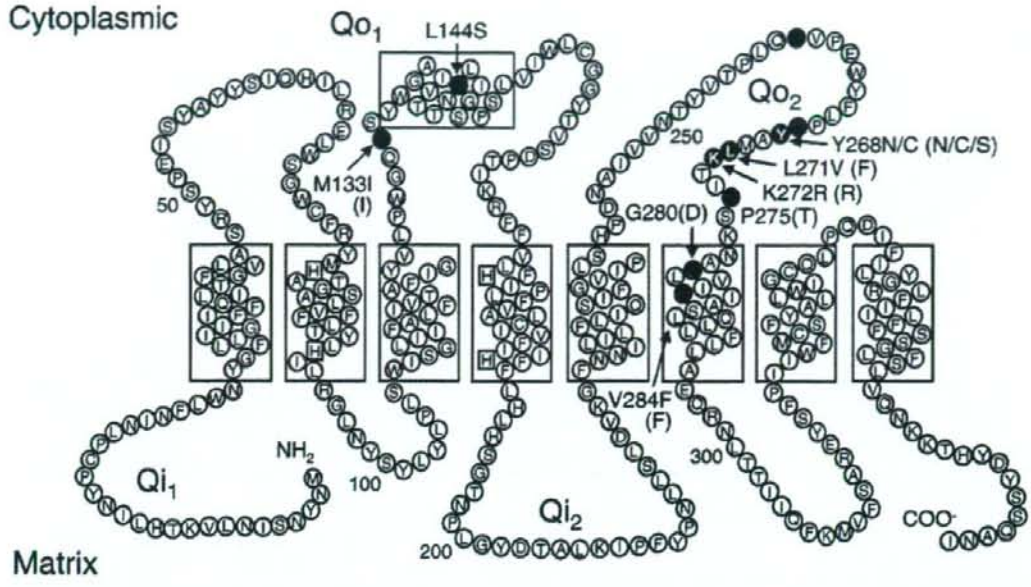

Fig. 1. Sites of atovaquone resistance mutations in the Qo_1 and Qo_2 domains of apocytochrome *b*. The apocytochrome *b* of *P. berghei* contains 376 amino acid residues and 8 transmembrane domains (boxed). Boxed "H"s are the universally conserved histidine residues that act as the axial ligands for b_{566} heme (H78 and H173) and b_{560} heme (H92 and H187). Shown are the four mutations identified in the present study, Y268N, Y268C, L271V, and K272R, all in the quinone binding site II (Qo_2) of the protein. The three atovaquone resistance mutations we reported previously [4] are indicated, M133I and L144S in the quinone binding site I (Qo_1), and V284F in the sixth transmembrane domain. Shown in brackets are mutations reported in *P. falciparum*, i.e. M133I, Y268S, Y268N, Y268C, L271F, K272R, P275T, G280D, and V284F [6,11,12] Other *Plasmodium* atovaquone resistance mutations that had been reported [5,7,8] are indicated as grey shaded residues; in *P. yoelii* these mutations are I258M, F267I, Y268C, L271V and K272R.

mutations (M133I and K272R or P275T), or in transmembrane V284K [6]. The atovaquone resistance conferred by these mutations were between 10 and 100 times lower than that of the field isolates carrying the Y268S mutation. The degree of resistance correlated well with the concentration of atovaquone used in the isolation, and may explain the absence of mutations in codon 268 *in vitro*.

Amino acid residues Y268 and L271 are highly conserved, indicating the potential importance of these residues in maintaining the cytochrome *b* structure and function. Residue 272, on the other hand, is a lysine in *Plasmodium* spp., but is an arginine in vertebrate proteins. Both Y268 and L271 have been suggested to be involved in atovaquone binding in *P. falciparum* cytochrome *b* [6]. Furthermore, in the yeast model [13,14], residues 279 and 282, equivalent to *Plasmodium* residues 268 and 271, have been predicted to be involved in the binding of atovaquone. Site-directed mutagenesis resulting in Y279S and L282V in yeast (corresponding to Y268S and L271V in *Plasmodium*) indeed conferred atovaquone resistance [14].

The two codon 268 mutations found in the present study, Y268N and Y268C, lead to significantly different degrees of resistance (ED_{50} 80 and 5.2, respectively). The aromatic side-chain of the tyrosine at residue 268 is important for the interaction between atovaquone and its binding pocket in the cytochrome *b* [13,14]; site-directed mutations in yeast that remove the aromatic chain gave rise to atovaquone resistance. The substitution of this large hydrophobic residue with the smaller asparagine or cysteine would affect this interaction, and the difference in the polarity of the side chains of the two amino acids could explain the difference in degree of resistance conferred.

We found in the present study that the mutation at codon 271 was always associated with either K272R or M133I. The single mutation, L271V, may lead to a functionally defective structure that requires compensative mutations, either in the adjacent Qo_2 site, 272, or in Qo_1 site, 133, to restore stability. The significantly reduced growth rates of the various atovaquone resistant mutants indeed suggest that there is some disruption of the cytochrome *b* function. The mutations in the atovaquone binding domain could for example affect also the functional interaction between coenzyme Q and the cytochrome *b*. Further biochemical analyses of the *P. berghei* atovaquone resistant clones are in progress to elucidate the structure functional relationship underlying atovaquone resistance, and to examine the fitness of the mutant strains in genetic crosses.

Acknowledgments

The authors wish to thank Dr. Andy Waters, Leiden University Medical Center (LUMC), Netherland, and Dr. A. Kurniawan, Dept. of Parasitology, Faculty of Medicine, University of Indonesia for the gift of *P. berghei* ANKA strains.

This work was supported by a grant from the Indonesian government through the Ministry of Research and Technology and from the Japan Society for the Promotion of Sciences (JSPS) to JES, through a JSPS fellowship for PhD RONPAKU program. This study was also supported by a grant-in-aid for scientific research on Priority Areas, for the 21st Century COE Program (F-3) and for Creative Scientific Research from the Japanese Ministry of Education, Science, Culture, Sports and Technology (180 73004, 18GS0314).

References

[1] Fry M, Pudney M. Site of action of the antimalarial hydroxynaphthoquinone, 2-[trans-4-(4'-chlorophenyl)cyclohexyl]-3-hydroxy-1,4-naphthoquinone(566C80). Biochem Pharmacol 1992;43:1545–53.

[2] Vaidya AB, Lashgari MS, Pologe LG, Morrisey J. Structural features of *Plasmodium* cytochrome *b* that may underline susceptibility to 8-aminoquinolines and hydroxynaphthoquinones. Mol Biochem Parasitol 1993;58:33–42.

[3] Srivastava IK, Rottenberg H, Vaidya AB. Atovaquone, a broad spectrum antiparasitic drug, collapses mitochondrial membrane potential in a malarial parasite. J Biol Chem 1997;272:3961–6.

[4] Syafruddin D, Siregar JE, Marzuki S. Mutations in the cytochrome *b* gene of *Plasmodium berghei* conferring resistance to atovaquone. Mol Biochem Parasitol 1999;104:185–94.

[5] Srivastava IK, Morrisey JM, Darrouzet E, Daldal F, Vaidya AB. Resistance mutations reveal the atovaquone-binding domain of cytochrome *b* in malaria parasites. Mol Microbiol 1999;33:704–11.

[6] Korsinczky M, Chen N, Kotecka B, Saul A, Rieckmann K, Cheng Q. Mutations in *Plasmodium falciparum* cytochrome *b* that are associated with atovaquone resistance are located at a putative drug-binding site. Antimicrob Agents Chemother 2000;44:2100–8.

[7] Walker DJ, Wakefield AE, Dohn MN, Miller RF, Baughman RP, Hossler PA, et al. Sequence polymorphism in the *Pneumocystis carinii* cytochrome *b* gene and their association with atovaquone prophylaxis failure. J Infect Dis 1998;178:1767–75.

[8] McFadden DC, Tomavo S, Berry EA, Boothroyd JC. Characterization of cytochrome *b* from *Toxoplasma gondii* and Q_o domain mutations as a mechanism of atovaquone-resistance. Mol Biochem Parasitol 2000;108:1–12.

[9] Fivelman QL, Butcher GA, Adagu IS, Warhust DC, Pasvol G. Malarone treatment failure and *in vitro* confirmation of resistance of *Plasmodium falciparum* isolate from Lagos, Nigeria. Malaria J 2002;1:1–4.

[10] David KP, Alifrangis M, Salanti A, Vestergaard LS, Ronn A, Bygbjerg IB. Atovaquone/proguanil resistance in Africa: a case report. Scand J Infect Dis 2003;35:897–8.

[11] Musset L, Bouchaud O, Matheon S, Massias L, Le BJ. Clinical atovaquone–proguanil resistance of *Plasmodium falciparum* associated with cytochrome *b* codon 268 mutations. Microbes Infect 2006;11:2599–604.

[12] Schwöbel B, Alifrangis M, Salanti A, Jelinek T. Different mutation patterns of atovaquone resistance to *Plasmodium falciparum in vitro* and *in vivo*: rapid detection of codon 268 polymorphisms in the cytochrome *b* as potential *in vivo* resistance marker. Malaria J 2003;2:1–7.

[13] Kessl JJ, Lange BB, Merbitz-Zahradnik TM, Zwickers K, Hill P, Meunier B, et al. Molecular basis for atovaquone binding to the cytochrome bc_1 complex. J Biol Chem 2003;278:31312–8.

[14] Kessl JJ, Ha KH, Merritt AK, Lange BB, Hill P, Meunier B, et al. Cytochrome *b* mutations that modify the ubiquinol-binding pocket of the cytochrome bc_1 complex and confer anti-malarial drug resistance in *Saccharomyces cerevisiae*. J Biol Chem 2005;280:17142–8.

A Cryptic Algal Group Unveiled: A Plastid Biosynthesis Pathway in the Oyster Parasite *Perkinsus marinus*

Motomichi Matsuzaki,[*1] *Haruko Kuroiwa,*[†] *Tsuneyoshi Kuroiwa,*[†] *Kiyoshi Kita,*[‡] *and Hisayoshi Nozaki*[*]

*Department of Biological Sciences, Graduate School of Science, University of Tokyo, Tokyo, Japan; †Department of Life Science, College of Science, and Research Information Center for Extremophile, Rikkyo University, Tokyo, Japan; and ‡Department of Biomedical Chemistry, Graduate School of Medicine, University of Tokyo, Tokyo, Japan

Plastids are widespread in plant and algal lineages. They are also exploited by some nonphotosynthetic protists, including malarial parasites, to support their diverse modes of life. However, cryptic plastids may exist in other nonphotosynthetic protists, which could be important in studies on the diversity and evolution of plastids. The parasite *Perkinsus marinus*, which causes mass mortality in oyster farms, is a nonphotosynthetic protist that is phylogenetically related to plastid-bearing dinoflagellates and apicomplexans. In this study, we searched for *P. marinus* methylerythritol phosphate (MEP) pathway genes, responsible for de novo isoprenoid synthesis in plastids, and determined the full-length gene sequences for 6 of 7 of these genes. Phylogenetic analyses revealed that each *P. marinus* gene clusters with orthologs from plastid-bearing eukaryotes, which have MEP pathway genes with essentially the same mosaic pattern of evolutionary origin. A new analytical method called sliding-window iteration of TargetP was developed to examine the distribution of targeting preferences. This analysis revealed that the sequenced genes encode bipartite targeting peptides that are characteristic of proteins targeted to secondary plastids originating from endosymbiosis of eukaryotic algae. These results support our idea that *Perkinsus* is a cryptic algal group containing nonphotosynthetic secondary plastids. In fact, immunofluorescent microscopy indicated that 1 of the MEP pathway enzymes, 1-deoxy-D-xylulose 5-phosphate reductoisomerase, was localized to small compartments near mitochondrion, which are possibly plastids. This tiny organelle seems to contain very low quantities of DNA or may even lack DNA entirely. The MEP pathway genes are a useful tool for investigating plastid evolution in both of the photosynthetic and nonphotosynthetic eukaryotes and led us to propose the hypothesis that ancestral "chromalveolates" harbored plastids before a secondary endosymbiotic event.

Introduction

"Plastids" are intrinsic organelles in plants and algae, but gaps remain in our knowledge regarding their diversity and distribution. Plastids originally arose from endosymbiotic cyanobacteria and are now involved in processes including photosynthesis and other biochemical processes in plant cells. Among the protists, several lines of algae or plastid-bearing eukaryotes (PBEs), such as giant kelp and diverse bloom-forming algae are known. Furthermore, intracellular parasites of the phylum Apicomplexa, including the malarial parasite, have been recently shown to harbor nonphotosynthetic but essential plastids (Wilson 2005). In a very recent environmental sequencing study, a distinct group of PBEs, the picobiliphytes, were discovered (Not et al. 2007). Thus, it seems very likely that unknown PBEs still exist.

On the basis of their deduced evolutionary history, plastids can be divided into 2 classes: primary plastids with 2 bounding membranes, which are direct descendants of endosymbiotic cyanobacteria, and secondary plastids with more bounding membranes, which originate from past engulfed eukaryotic algae (Bhattacharya et al. 2004). Because secondary plastids remain "outside" with regard to membrane topology, proteins targeted to these compartments must be transported via a secretory pathway; they must contain an N-terminal bipartite targeting peptide, composed of a signal peptide (SP) to lead the polypeptide to the endoplasmic reticulum (ER), and a subsequent transit peptide (TP) to deliver the mature protein into the plastid lumen (van Dooren et al. 2001). Secondary PBEs are scattered over the protist phylogeny; however, it has been proposed that members of the so-called chromalveolate group, which consists of diatoms and other stramenopiles, haptophytes, cryptophytes, dinoflagellates, and apicomplexans, ancestrally contain secondary plastids of a single red algal origin (Cavalier-Smith 1999). Several lines of "evidence" support the "chromalveolate" hypothesis (Fast et al. 2001; Yoon et al. 2002), but critics note that the hypothesis assumes too many independent losses of plastids (Body† 2005). Thus, a better understanding of plastid distribution in the basal chromalveolates is desirable to address these criticisms.

Perkinsus spp. are marine unicellular protists with a worldwide distribution that attack a wide range of mollusks, including clams and abalones, causing mass mortality (Villalba et al. 2004). *Perkinsus marinus* is the most notorious species of the genus because it parasitizes the eastern oyster *Crassostrea virginica* and has heavily impacted oyster fisheries and hence coastal water quality in the United States (Villalba et al. 2004). Molecular phylogenetic data have shown that this species is a basal chromalveolate derived from the ancestral dinoflagellates just after the split from apicomplexans (Cavalier-Smith and Chao 2004; Leander and Keeling 2004; Adl et al. 2005); thus, examining *P. marinus* for the existence of ancestral secondary plastids is of interest. Although electron microscopy (EM) observations have revealed no signs of plastids (Perkins and Menzel 1967; Perkins 1976, 1996; Sunila et al. 2001), 2 quite recent studies have suggested that *Perkinsus* spp. contain secondary plastids; *P. marinus* was shown to possess genes for a plant-type ferredoxin system that possibly encode plastid-targeting signals (Stelter et al. 2007) and an EM observation indicated a tiny organelle bounded by 4 membranes in *Perkinsus olseni* (=*Perkinsus*

[1] Present address: Department of Biomedical Chemistry, Graduate School of Medicine, University of Tokyo, Tokyo, Japan.

Key words: secondary endosymbiosis, protein sorting signal, chromalveolates, methylerythritol phosphate pathway, *Perkinsus marinus*.

E-mail: mzaki@m.u-tokyo.ac.jp

Mol. Biol. Evol. 25(6):1167–1179. 2008
doi:10.1093/molbev/msn064
Advance Access publication March 20, 2008

atlanticus) (Teles-Grilo et al. 2007). However, gene sequence or morphology in itself cannot prove the existence of vestigial plastids; at the least, localization data should be presented in order to confirm the presence of plastids.

Genome sequencing has revealed that biosynthesis of isoprenoid precursors is a key metabolic role of both photosynthetic (Matsuzaki et al. 2004; Derelle et al. 2006) and nonphotosynthetic (Gardner et al. 2002, 2005) plastids. Isoprenoids are a diverse and versatile group of compounds including sterols, carotenoids and other terpenes, and the side chains of quinones and chlorophylls. Isoprenoids are all derived from isopentenyl diphosphate and its isomer, both of which are synthesized by the methylerythritol phosphate (MEP) pathway in plastids but the mevalonate (MVA) pathway in the cytosol of many eukaryotes, including higher plants and animals (Rodríguez-Concepción 2004). It has been suggested that in eukaryotes the MEP pathway only exists in PBEs, with a discussion of the evolutionary origins of the genes based on the orthologs of higher plants and several bacteria, although only 5 out of 7 MEP genes were known at the time (Lange et al. 2000). Many eukaryotic genomes have been sequenced since then, and to date the MEP pathway genes have been found to be specific to PBEs and would seem to be necessary for most given that they lack the MVA pathway genes; thus, it seems that the MEP pathway is a specific feature of plastids, photosynthetic, or otherwise. Therefore, the 7 MEP pathway genes (shown in fig. 1) would be good molecular markers for the study of plastid distribution and evolutionary history; however, to the best of our knowledge, no prior studies have involved the widespread sampling of PBEs.

A preliminary database of the *P. marinus* genome at The Institute for Genomic Research (TIGR) contains partial sequences of the MEP pathway genes (the existence of ispC, ispG, and ispH has already been discussed by Stelter et al. [2007]). In this study, we attempted to clone full-length MEP pathway genes of *P. marinus* to elucidate the evolution of secondary plastids by phylogenetic analyses. A new analytical method for investigating protein sorting signals was also developed to compare signals between genes. Finally, immunofluorescent microscopy was performed to demonstrate the existence of plastids in *P. marinus*.

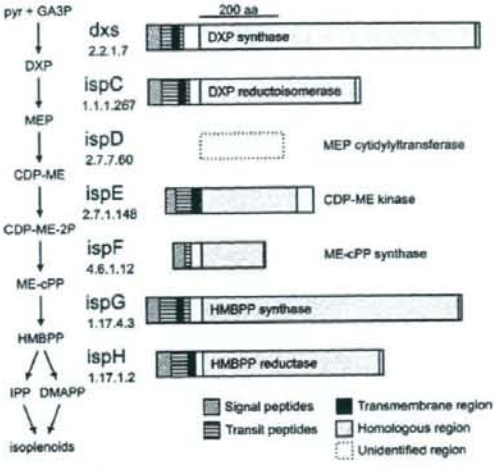

FIG. 1.—The MEP pathway and responsible genes in *Perkinsus marinus*. The flowchart on the left shows the compounds and reactions involved in the MEP pathway, with the name of the gene responsible and an Enzyme Committee number listed for each reaction. Compounds are abbreviated as follows: pyr, pyruvate; GA3P, glyceraldehyde 3-phosphate; DXP, 1-deoxy-D-xylulose 5-phosphate; MEP, 2-*C*-methyl-D-erythritol 4-phosphate; CDP-ME, 4-diphosphocytidyl methylerythritol; CDP-ME-2P, CDP-ME 2-phosphate; ME-cPP, methylerythritol 2,4-cyclodiphosphate; HMBPP, 1-hydroxy-2-methyl-2-butenyl 4-diphosphate; IPP, isopentenyl diphosphate; and DMAPP, dimethylallyl diphosphate. On the right are schematic representations of the inferred structures of MEP pathway enzymes in *P. marinus*. N-terminal extensions that were putatively composed of SP (diagonal hatch) and TP (horizontal stripe) with a transmembrane region (filled) were located next to the regions that were homologous to each enzyme's bacterial counterpart (shaded). The gene for the third step, an *ispD* ortholog, is unidentified and indicated by a box with dotted edges. The scale is indicated at the top of the figure.

Materials and Methods

Culture Conditions

Perkinsus marinus strain CRTW-3HE was obtained from the American Type Culture Collection (number 50439; ATCC, Manassas, VA) and maintained at 26 °C in ATCC Medium 1886. Discontinued products for the medium components were substituted as follows during the course of the study: Instant Ocean Sea Salt (Aquarium Systems, Mentor, OH) for artificial seawater (S1649; Sigma, St Louis, MO) and Lipid Mixture (1000×; L5146; Sigma) for Lipid Concentrate (100×; 21900-014; Gibco, Grand Island, NY).

Sequencing MEP Pathway Genes

Total RNA was extracted from cell pellets using TRIzol Reagent (Invitrogen, Carlsbad, CA), and the mRNA was enriched using the PolyATtract mRNA Isolation System III (Promega, Madison, WI). Complementary DNA was synthesized using the CapFishing Full-length cDNA Premix Kit (Seegene, Seoul, Korea) with random hexamers or the oligo dT adapter as a primer. Reverse transcriptase–polymerase chain reaction and rapid amplification of cDNA ends were performed using PrimeSTAR HS DNA polymerase (Takara Bio, Tokyo, Japan) and the primers listed in supplementary table S1 (Supplementary Material online). Polymerase chain reaction products were purified using Wizard SV Gel and PCR Clean-Up System (Promega) and then cloned with the ZeroBlunt TOPO PCR Cloning Kit for Sequencing (Invitrogen). Inserts were sequenced using vector-specific or gene-specific (shown in supplementary table S1, Supplementary Material online) primers. Full-length sequences have been deposited in DDBJ/EMBL/GenBank under the accession numbers AB284361–AB284366 (shown in supplementary table S3, Supplementary Material online). All experiments described here were performed according to the manufacturers' instructions. The amino acid sequences were inferred from the most upstream ATG with the universal codon table.

Phylogenetic Analysis

All possible MEP pathway orthologs for bacteria for which complete genome sequences were available as of 1

November 2006 were retrieved from the National Center for Biotechnology Information Refseq database. Very large multiple sequence alignments were constructed using MUSCLE 3.6 (Edgar 2004) and then 50 bacteria were chosen (supplementary table S2, Supplementary Material online) based on the alignments to retain at least a single species for each bacterial phylum and to eliminate species with organism-specific indels when possible. Amino acid sequences for 8 eukaryotes were deduced based on the sequenced genome databases (supplementary table S3, Supplementary Material online). Data matrices were constructed as follows: structure-based alignments were created for bacterial sequences using the Expresso (Armougom et al. 2006) Web service (http://www.tcoffee.org/), then eukaryotic sequences were added using ClustalX 1.83 (Thompson et al. 1997), and the results were manually refined and sites chosen for analysis. Although the Expresso Web service was used, ispG and ispH alignments were constructed by conventional methods because no suitable structural data were available for these genes. First, maximum likelihood (ML) trees were inferred with a WAG substitution matrix (Whelan and Goldman 2001) using Phyml 2.4.4 (Guindon and Gascuel 2003) with bootstrap values (100 replications), and distant problematic bacterial sequences (underlined in supplementary table S2, Supplementary Material online) were eliminated. Final ML trees were then inferred within additional operational taxonomic units (OTUs) for dinoflagellates and haptophytes, which have been obtained and synthesized from expressed sequence tags (EST) (source organisms and the original accession numbers are shown in the supplementary table S3, Supplementary Material online). Apicomplexan orthologs were excluded because they contain a vast number of changed or inserted residues, making it difficult to robustly infer phylogeny. In fact, trees drawn to include them resulted in placing them at deeper branches, disturbing tree topology, or reducing statistical support to greater or lesser degrees (data not shown).

Targeting Presequence Analysis

The N-terminal extensions of the translated amino acid sequences for each MEP pathway gene were examined using SignalP-HMM (Nielsen and Krogh 1998; Bendtsen et al. 2004) for SP and SOSUI (Hirokawa et al. 1998) for the transmembrane region. The distribution of protein sorting signals was examined using newly developed sliding-window iteration of TargetP (SWIT) analysis. Amino acid sequences were inferred from the first in-frame start codon, and subcellular localization was predicted by submitting the first 130 residues to the TargetP server (http://www.cbs.dtu.dk/services/TargetP/) (Nielsen et al. 1997; Emanuelsson et al. 2000); this was then repeated successively after eliminating the first residue from the N-terminus of the previously analyzed amino acid sequence (i.e., sliding a 130-residue window with a 1-residue step). Iterations were performed using the newly developed Ruby script, facilitated by the BioRuby library (http://www.bioruby.org/) (Goto et al. 2003). TargetP yields scores for SP, mitochondrial TP (mTP), chroloplast TP (cTP), and an other category for each iteration. The 4 scores were plotted with window positions on the y and x axes. Two superoxide dismutase genes, PmSOD1 and PmSOD2 (AY095212 and AY095213, respectively), were used for comparison (Wright et al. 2002).

Antibody

Rabbits were immunized with 2 synthesized peptides, TATVEDALKHPNWS and YTLAYPQRLHHDGS, which were partial fragments of the deduced ispC peptide sequence. A fraction of IgG (270 μg/ml) from the sera was obtained by affinity purification using the peptide cocktail to capture specific antibody. Recombinant ispC protein (with an N-terminal 6×His tag) lacking the predicted bipartite targeting peptide was expressed in *Escherichia coli* BL21-AI (Invitrogen) and was purified using HisTrap FF crude (GE Healthcare, Little Chalfont, Buckinghamshire, UK). We discovered that the cytosolic fraction of *P. marinus* contained a protein that nonspecifically reacted with normal rabbit IgG (Santa Cruz Biotechnology, Santa Cruz, CA); therefore, all antibodies were first adsorbed with proteins from the cytosolic fraction of *P. marinus* that were obtained by precipitation with 50–70% saturated ammonium sulfate.

Centrifugal Fractionation

Cells were collected by centrifugation (200 × g for 5 min at ambient temperature), washed with phosphate-buffered saline (PBS), resuspended in 50 mM *N*-2-hydroxyethylpiperazine-*N'*-2-ethanesulfonic acid buffer (pH 7.4) supplemented with protease inhibitor cocktail (Complete; F. Hofmann-La Roche, Basel, Switzerland), and disrupted by sonication on ice. The homogenate was subjected to differential centrifugal fractionation at 4 °C and divided into 4 fractions: 200 × g sediment (5 min), 2,000 × g sediment (10 min), 20,000 × g sediment (15 min), and the supernatant. The 20,000 × g sediment was incubated for 30 min at 4 °C in buffer containing 0.5% Triton X-100 and was then centrifuged at 20,000 × g for 15 min. All fractions were subjected to western blotting performed according to the following protocol: proteins separated by sodium dodecyl sulfate–polyacrylamide gel electrophoresis (10% gel) were transferred to PVDF membrane (Immobilon-P; Millipore, Billerica, MA), membranes were blocked for 1 h in blocking buffer (3% bovine serum albumin and 0.05% Tween 20 in PBS), and primary antibody (1:1000 dilution of the affinity-purified antibody) was added for 1 h. Next, alkaline phosphatase-conjugated Goat Anti-Rabbit IgG (Fc) (Promega S3731) in blocking buffer (1:7500) was added for 1 h and then the blots were developed by addition of BCIP/NBT Color Development Substrate (Promega S3771).

Immunofluorescent Microscopy

Cells were incubated for 30 min in culture medium containing 200 nM CMXRos (MitoTracker Red; Invitrogen M7512), washed for 15 min, and then fixed for 30 min at

−20 °C with 4% (w/v) paraformaldehyde in 85% (v/v) methanol. Fixed cells were washed with PBS and then mounted on Matsunami adhesive silane–coated slides (Matsunami Glass Industries, Kishiwada, Japan) and air dried. The slides were blocked for 1 h with BlockAce (Dainippon Sumitomo Pharma, Osaka, Japan) containing 4 μg/ml normal goat IgG (Santa Cruz Biotechnology), labeled for 1 hr with a 1:1000 dilution of affinity-purified antibody, and then incubated for 1 h with 1:400 dilution of Alexa Fluor 488 Goat Anti-Rabbit IgG (H + L; Invitrogen A11008) in Can Get Signal immunostain Solution A (Toyobo, Osaka, Japan). After counterstaining with 1 μg/ml 4′,6-diamidino-2-phenylindole (DAPI), the slides were observed under an epifluorescence microscope (Olympus BX60) equipped with cooled digital color camera (Olympus DP70). For negative control experiments, the affinity-purified antibody was omitted or substituted with the same concentration of normal rabbit IgG.

Results

MEP Pathway Genes

We first searched for MEP pathway genes using a similarity search service at the *P. marinus* genome database of TIGR (http://www.tigr.org/tdb/e2k1/pmg/) using red alga, green alga, and apicomplexan homologs as queries for each gene (identifiers are shown in supplementary table S3, Supplementary Material online). Irrespective of species used as queries, all homologs resulted in the same significant hits: single contigs for *dxs*, *ispC*, *ispE*, and *ispF* and 2 contigs for *ispG* and *ispH*. For the latter genes, the hits were located at the termini of contigs and were assumed to be single genes astride contig gaps. Thus, all these genes were thought to exist only in single copy. In contrast, MVA pathway genes were not found when we searched for them in a similar fashion.

Six out of 7 MEP pathway genes (fig. 1) were then sequenced in their entirety using gene-specific primers designed based on the contig sequences. No homolog of the gene responsible for the third step, *ispD*, was found in the database, and an attempt to amplify the gene using degenerate primers failed. Untranslated regions were short, 19–45 and 15–97 nt for the 5′ and 3′ ends, respectively.

Evolutionary Origin and Relationships

To investigate the evolutionary origin of the sequenced MEP pathway genes, we performed phylogenetic analyses using PBEs and a wide range of bacteria. The dxs ortholog of *P. marinus* clusters with those of PBEs, and they form a clade with the alpha-proteobacterial counterparts with 100% bootstrap support, which is independent of cyanobacterial orthologs (fig. 2). The ispC orthologs of *P. marinus* and PBEs form a clade with the cyanobacterial orthologs with 100% bootstrap support (fig. 3). For the ispE tree, eukaryotic orthologs, including that of *P. marinus* and chlamydial counterparts, form a weakly supported (76%) clade (fig. 4). The ispF ortholog of *P. marinus* clusters with those of PBE with weak bootstrap support (58%), but the clade has failed to show a relationship with specific

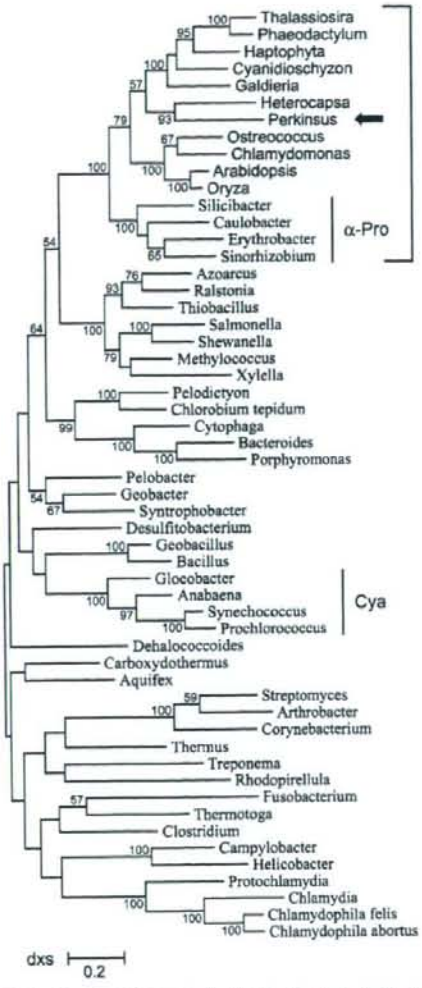

FIG. 2.—Unrooted ML tree for dxs (log likelihood = −35,861.100656) constructed using Phyml with WAG substitution matrix, based on a matrix comprising 55 OTUs and 497 sites. OTU names in sans serif indicate they are eukaryotic orthologs, and the bold arrow denotes the *Perkinsus marinus* ortholog. Haptophyta OTU is a synthetic sequence composed of *Emiliania*, *Isochrysis*, and *Pavlova* ESTs (supplementary table S3, Supplementary Material online) and lacks 23% of sites. Heterocapsa OTU is also a synthetic sequence derived from ESTs and lacks 6% of sites. Cyanobacterial (Cya) and alpha-proteobacterial (α-Pro) orthologs are indicated. Numbers adjacent to the nodes indicate bootstrap support (100 replicates), and values below 50% have been omitted. The scale bar indicates the number of substitutions per site.

bacteria (fig. 5). This is probably because of the shorter data matrix (104 sites), corroborated by poor phylogenetic resolution of the overall tree. For the ispG tree, the *P. marinus* ortholog and eukaryotic orthologs other than those from red algae form a clade with the chlamydial orthologs with 100% bootstrap support, whereas red algal orthologs form another clade with the cyanobacterial orthologs (fig. 6). The

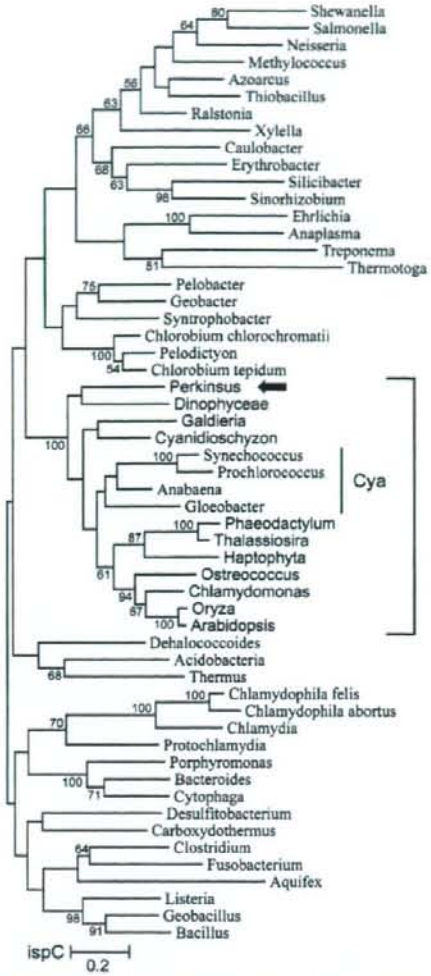

FIG. 3.—Unrooted ML tree for ispC (log likelihood = −25,588.615193) constructed using Phyml with WAG substitution matrix, based on a matrix comprising 55 OTUs and 337 sites. Haptophyta and Dinophyceae OTUs are synthetic sequences composed of *Emiliania* and *Isochrysis* ESTs, and *Alexandrium* and *Crypthecodinium* ESTs (supplementary table S3, Supplementary Material online), and lack 13% and 31% of sites, respectively. Cyanobacterial (Cya) orthologs are indicated. See also the legend of figure 2.

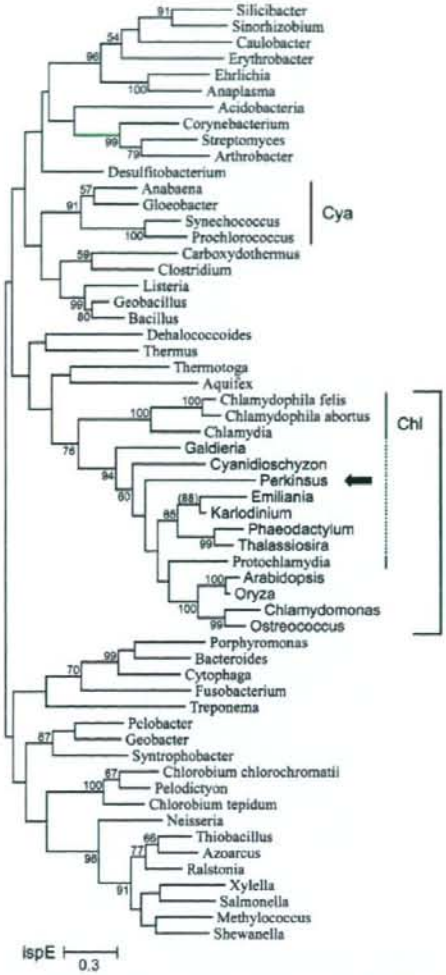

FIG. 4.—Unrooted ML tree for ispE (log likelihood = −16,236.630250) constructed using Phyml with WAG substitution matrix, based on a matrix comprising 58 OTUs and 175 sites. Emiliania and Karlodinium OTUs are partial sequences derived from ESTs (supplementary table S3, Supplementary Material online), lack 50% and 54% of sites, respectively, and do not overwrap; therefore, it could be an artifact that they form a clade although with a high bootstrap value (88, as indicated in parentheses). Cyanobacterial (Cya) and chlamydial (Chl) orthologs are indicated. See also the legend of figure 2.

ispH orthologs of *P. marinus* and PBEs form a clade with the cyanobacterial orthologs with 100% bootstrap support (fig. 7). All these results indicate that each of *P. marinus* orthologs clusters with the corresponding PBE orthologs; thus, the *P. marinus* orthologs are unlikely to have been independently transferred from bacteria.

Some of the *P. marinus* orthologs showed weak phylogenetic affinity to the dinoflagellate orthologs. The dxs ortholog formed a highly supported clade with the dinoflagellate *Heterocapsa* (fig. 2). The ispC ortholog formed a clade with a synthetic dinoflagellate OTU with <50% bootstrap support (fig. 3). Additionally, when a short sequence (105 sites) from the dinoflagellate *Amphidinium* ortholog was included in the ispG analysis, it was sister to the *Perkinsus* ortholog but with weak bootstrap support (54%). However, bootstrap supports for the adjacent nodes became weak, possibly due to the short dinoflagellate sequence (data not shown). The statistical weakness seems attributed to missing data derived from using partial ESTs of the dinoflagellate orthologs. In fact, the dxs tree, which has

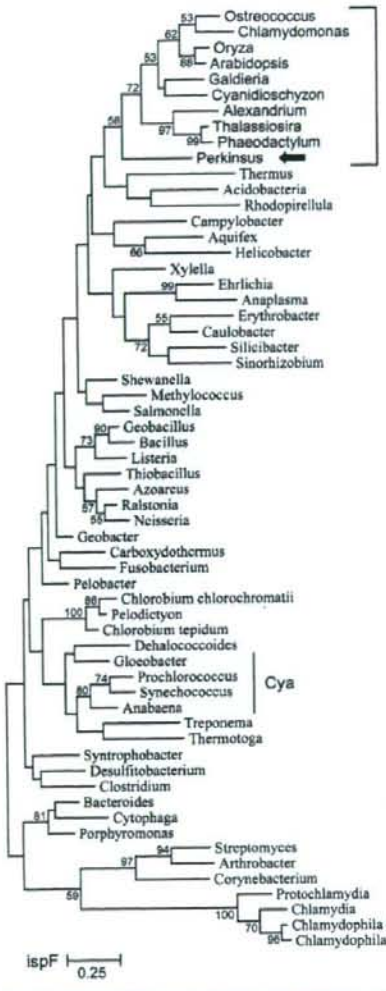

FIG. 5.—Unrooted ML tree for ispF (log likelihood = −7,405.683963) constructed using Phyml with WAG substitution matrix, based on a matrix comprising 60 OTUs and 104 sites. Alexandrium OTU is a partial sequence derived from ESTs (supplementary table S3, Supplementary Material online) and lacks 11% sites. Cyanobacterial (Cya) orthologs are indicated. See also the legend of figure 2.

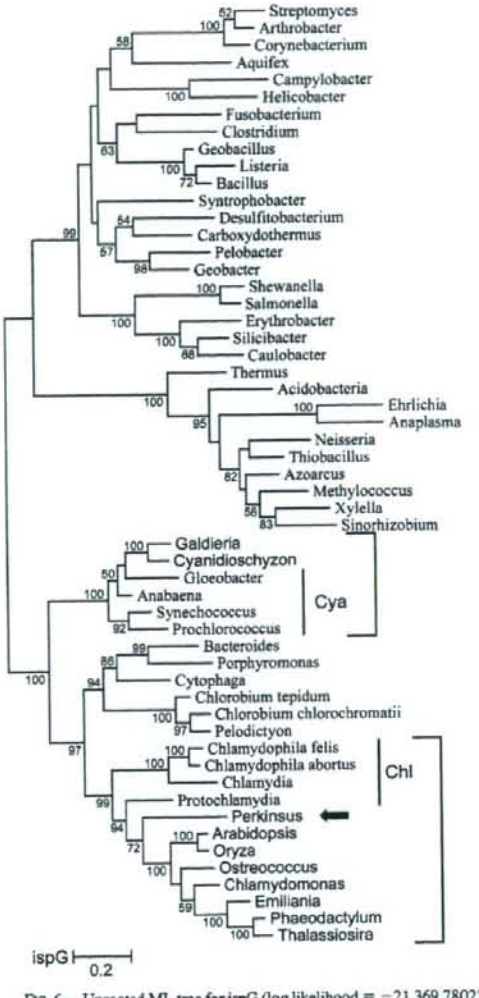

FIG. 6.—Unrooted ML tree for ispG (log likelihood = −21,369.78023) constructed using Phyml with WAG substitution matrix, based on a matrix comprising 55 OTUs and 344 sites. Emiliania OTU is a synthetic sequence derived from ESTs (supplementary table S3, Supplementary Material online). Amphidinium OTU was excluded because it was derived from a short EST and lacked 70% of sites; however, it was sister to the *Perkinsus* ortholog with weak (54%) bootstrap support when it was included in the matrix. Cyanobacterial (Cya) and chlamydial (Chl) orthologs are indicated. See also the legend of figure 2.

the strongest support, has the lowest amount of missing data (6% of sites) in the dinoflagellate ortholog. Therefore, the strength of this phylogenetic model may improve if full-length sequences become available. Reliable relationships for ispE and ispF orthologs of *P. marinus* were not resolved, and this was probably due to long-branch attraction or the shorter data matrix (figs. 4 and 5). The ispE tree (fig. 4) shows a highly supported close relationship between orthologs of the haptophyte *Emiliania* and the dinoflagellate *Karlodinium*. Although *Karlodinium* has a tertiary plastid derived from haptophytes, the close relationship should not be interpreted as a result of endosymbiotic gene transfer, but rather as an artifactual grouping of stray OTUs, because these 2 OTUs are derived from partial ESTs and have no overwrap on the sequence alignment. To summarize, in total, the MEP pathway genes of *P. marinus* have weak phylogenetic affinity to those of dinoflagellates, and this likely shows that the MEP pathway is descended from the common ancestor of *P. marinus* and dinoflagellates.

The present phylogenetic trees indicate that the MEP pathway genes of PBEs and *P. marinus* have essentially the

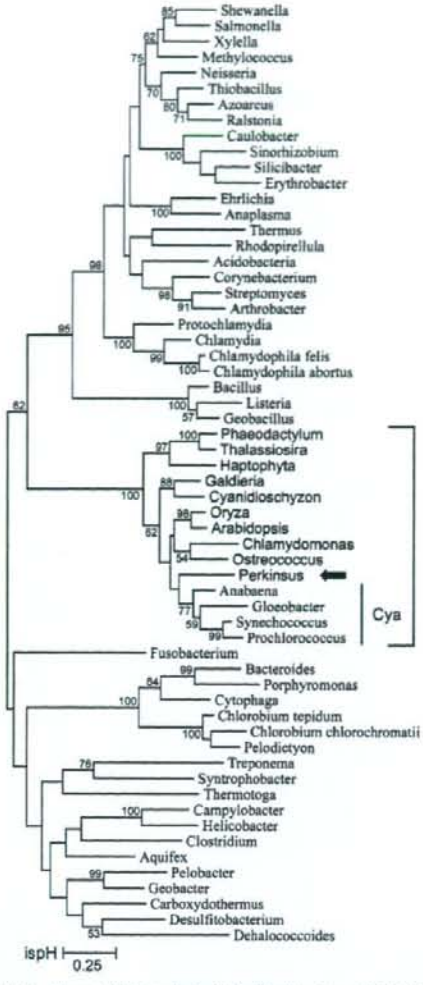

FIG. 7.—Unrooted ML tree for ispH (log likelihood = −18,623.672548) constructed using Phyml with WAG substitution matrix, based on a matrix comprising 60 OTUs and 230 sites. Haptophyta OTU is a synthetic sequence composed of *Emiliania* and *Pavlova* ESTs (supplementary table S3, Supplementary Material online) and lacks 10% of sites. Cyanobacterial (Cya) orthologs are indicated. See also the legend of figure 2.

same pattern of mosaic origins in Cyanobacteria, Proteobacteria, and Chlamydia (table 1). In PBEs, dxs (fig. 2) and ispE (fig. 4) had a sister relationship with the proteobacterial and chlamydial orthologs, respectively, whereas ispC and ispH seemed to be derived from Cyanobacteria (figs. 3 and 7). A chlamydial origin was also observed for ispD orthologs (supplementary fig. S1, Supplementary Material online). The evolutionary origin of ispF remains unclear, probably owing to insufficient informational sites being used (fig. 5). However, only red algae had cyanobacteria-like ispG orthologs, and *P. marinus* and other PBEs

Table 1
Shared Mosaic Origins of MEP Pathway Genes

	dxs	*ispC*	*ispD*	*ispE*	*ispF*	*ispG*	*ispH*
Green plants	pro	cya	chl	chl?	#	chl	cya
Red algae	pro	cya	chl	chl?	#	cya	cya
Diatoms	pro	cya	chl	chl?	#	chl	cya
Haptophytes	pro	cya	chl	chl?	—	chl	cya
Dinoflagellates	pro	cya	chl	chl?	#	chl?	—
Perkinsus	pro	cya	—	chl?	#	chl	cya

NOTE.—chl, chlamydia; cya, cyanobacteria; pro, α-proteobacteria; —, not found; ?, supported with weak bootstrap values; and #, monophyletic but showing no clear relationships.

harbored genes that were closely related to their chlamydial counterparts (fig. 6). This difference is not a phylogenetic artifact because there were long and well-aligned insertion sequences that were shared with PBEs other than red algae and Chlamydia (supplementary fig. S2, Supplementary Material online). The present phylogenetic analyses demonstrated that *P. marinus* and all PBEs analyzed here, with a curious exception of red algae, obtained their MEP pathway genes from an identical source.

Targeting Presequence and Subcellular Localization

The inferred amino acid sequences of the 6 MEP pathway genes in *P. marinus* have obvious N-terminal extensions relative to their bacterial homologs (fig. 1). N-terminal extensions often function as targeting presequences to deliver the peptide into certain subcellular compartments (e.g., ER, mitochondria, and plastids). First, SignalP predicted that all genes would have SPs (fig. 1; supplementary fig. S3, Supplementary Material online), although the probability of cleavage was not very high. Each predicted SP indicated an abnormally long (10–20 residues) hydrophilic n-region, but h- and c-regions were normal (supplementary fig. S3, Supplementary Material online). Because elimination of a few residues from the N-termini of the n-regions greatly improved the cleavage probability (data not shown), we consider that SPs with minor modification exist and they are likely cleaved off. The cleavable SP indicates that the MEP pathway enzymes are trafficked via the secretory pathway. However, TargetP predicted that all MEP pathway orthologs (except dxs) would be targeted to mitochondria. A lesson learned from the SignalP result is that simple predictions using full-length sequences may yield dubious results if the organism under question is distantly related to organisms after which the predictor has been modeled. Therefore, the need exists to monitor trends and the robustness of results obtained by TargetP analysis to better understand whether the mitochondrial targeting was significant and to further investigate the characteristics of the N-terminal extension.

We developed a new method of exploiting TargetP in order to robustly examine the distribution of targeting preferences. The method iteratively invoked TargetP with a sliding 130-residue window from the N-terminus; thus, we named the method SWIT. Figure 8 shows the SWIT results for the MEP pathway genes and 2 *P. marinus* superoxide dismutases, PmSOD1 and 2 (Wright et al. 2002). For

example, for dxs, a prediction with the first 130 residues yielded scores of 0.002, 0.062, 0.165, and 0.064 for cTP, mTP, SP, and others (*y* intercepts for green, blue, yellow, and gray lines), respectively; this is equivalent to the simple TargetP prediction using the full-length sequence. As the window slides downstream, the SP score increases up to 0.393 and then decreases to near zero. Although the first result (*y* intercept) alone, or the simple TargetP prediction, seems rather unreliable, we recognize that the N-terminal region likely has SP preference (yellow arrow). As the window slides along, a significant prominence for cTP appears (green arrow) in the vicinity of the predicted SP cleavage site (yellow triangle). The MEP pathway genes shared this characteristic SWIT trend, that is, a peak in the SP score at the N-terminal region and a subsequent increase in the cTP score. The trends seem to suggest that these enzymes are localized to secondary plastids because an N-terminal bipartite (SP + cTP) presequence is a characteristic feature of proteins of secondary plastids (van Dooren et al. 2001). Thus, we hypothetically considered residues between the N-terminus and the predicted SP cleavage site and between the SP cleavage site and the most downstream predicted site for cTP cleavage (green triangles) as putative SP and cTP, respectively.

One issue is that all aforementioned genes, except dxs, have considerable mTP scores at the *y* intercepts (fig. 8), which correspond to the simple TargetP results (see above). Both PmSOD1 and 2 also have high mTP scores at their N-termini, similar to the 5 MEP pathway genes (fig. 8); however, PmSOD2 localizes to an unknown, nonmitochondrial compartment, whereas PmSOD1 localizes to the mitochondria (Schott and Vasta 2003). According to the SWIT result, the mTP score for PmSOD1 is maintained along the N-terminal extension, and this corresponds to its mitochondrial localization; however, the score for PmSOD2 rapidly declines and SP and subsequent cTP preferences appear alternatively. Given that SP and cTP preferences do not appear for PmSOD1, they can be used to discriminate localization to a compartment other than the mitochondria; additionally, a high mTP score at the N-terminus has no biological significance when there are significant SP and cTP preferences. The MEP pathway genes share the SP + cTP feature with PmSOD2; thus, the MEP pathway genes appear to have protein sorting signals that are characteristic of proteins targeted to secondary plastids and to be localized to a compartment other than the mitochondria.

The predicted TP regions suggested by SWIT analysis were further examined in comparison to the TPs of PBEs. The predicted regions were overall hydrophilic and with a net positive charge, as in PBEs, resulting from depletion of acidic residues (5.3% compared with 12.9% in the homologous region) and accumulation of hydroxylated residues (especially Ser; 16.2% compared with 6.4%) and positive-charged residues (especially Arg; 7.1% compared with 5.2%). All but ispF were shown to possess Phe residues in a hydrophobic context in proximity to the SP cleavage site, and a single transmembrane helix followed by an Arg-rich region within the TP region (fig. 1; supplementary fig. S3, Supplementary Material online). This feature resembles a similar feature in the class I TP of peridinine dinoflagellates, and no apicomplexans reported so far harbor

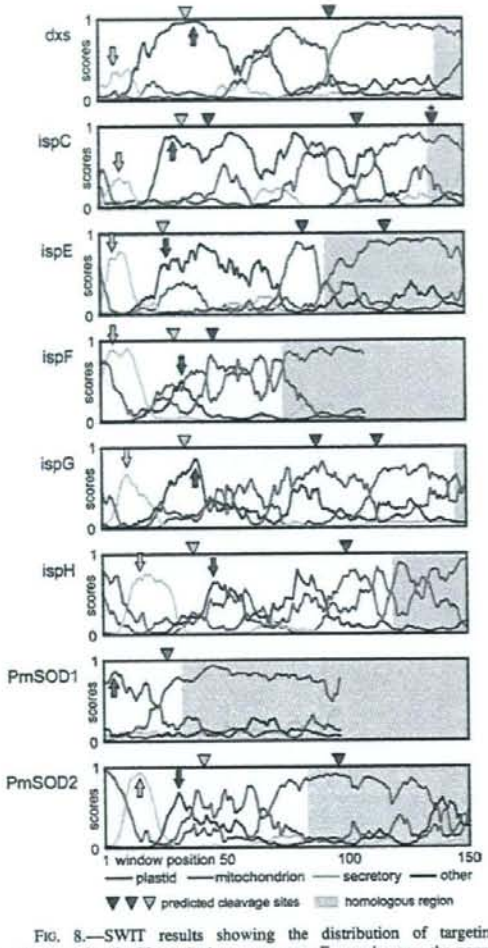

FIG. 8.—SWIT results showing the distribution of targeting preferences for the N-terminal presequences. For each gene, the neural network scores (*y* axis) of the TargetP prediction are plotted for the N-terminal 150 amino acids (*x* axis) in the following colors: green, plastid TP; light blue, mitochondrial TP; yellow, SP for secretory pathway; and gray, other location. Thus, the *y* intercepts correspond to the simple TargetP predictions. Triangles above each plot indicate the predicted cleavage sites: green, sites for plastid TP that appeared in the SWIT analysis; light blue, sites for mitochondrial TP (only for PmSOD1); and yellow, sites for SP as predicted by SignalP-HMM. The homologous region is shown in gray on each plot.

the transmembrane helix (Patron et al. 2005). No hydrophobic regions were predicted for ispF or PmSOD2, which makes them similar to the class II TP on the other hand (Patron et al. 2005). Collectively, the predicted TP regions resemble those of the peridinine dinoflagellates with respect to physicochemical features and class duality.

To examine whether the predicted bipartite targeting sequence is functional, a polyclonal antibody recognizing the second step enzyme coded by *ispC* was prepared. The affinity-purified antipeptide antibody successfully detected recombinant ispC (fig. 9*A*, lane 1), and it detected

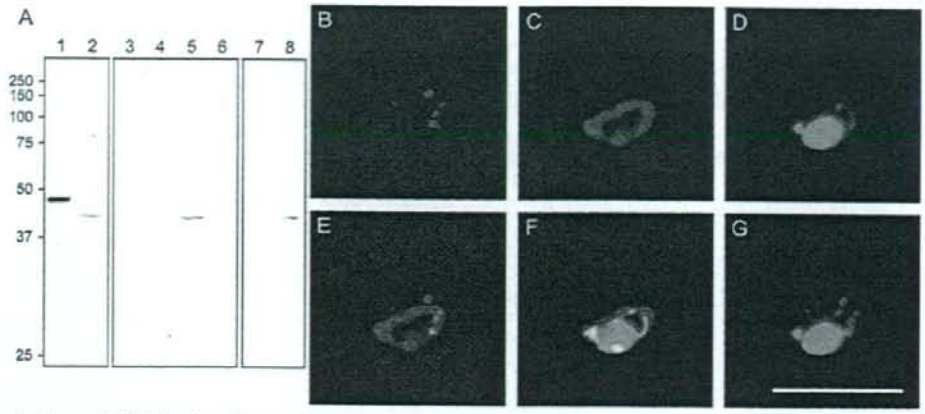

FIG. 9.—Immunological detection of the second step enzyme ispC. (*A*) Fractionation experiments for ispC. The size of ispC can be seen in lanes 1 and 2; a His-tagged recombinant ispC protein (1) acts as a positive control, and *Perkinsus marinus* cell lysate (2) contains native ispC. Lanes 3–6 show centrifugal fractionation of homogenized cell lysate; equivalent amounts of the 200 × g sediment (3), 2,000 × g sediment (4), 20,000 × g sediment (5), and 20,000 × g supernatant (6) were applied. Lanes 7 and 8 show the effect of Triton X-100 treatment on the 20,000 × g sediment (5); equivalent amounts of the 20,000 × g sediment (7) and 20,000 × g supernatant (8) were applied. Immunofluorescent microscopy indicating localization of ispC (*B–G*). Alexa Fluor 488 signals labeling ispC (*B*), CMXRos signals indicating mitochondria (*C*), and DAPI signals indicating DNA (*D*) were obtained from the same visual field. An overlaid image of ispC and mitochondria (*E*) indicates that the ispC protein localizes to punctate compartments near mitochondria. Those of DNA and mitochondria (*F*), and DNA and ispC (*G*) indicate that the mitochondria definitely contain DNA but the putative plastids do not contain detectable amounts of DNA. Bar indicates 10 μm.

a protein of approximately 43 kDa in *P. marinus* cell lysates (lane 2). Although smaller in size than predicted molecular weight of ispC (51 kDa), the size corresponds to an estimated molecular weight of the mature protein after cleavage of the predicted bipartite targeting peptides (asterisk in fig. 8). Detection at 43 kDa suggests that ispC is transported using targeting peptides that are subsequently cleaved. SOSUI predicted that the mature ispC protein was soluble. However, centrifugal fractionation showed the ispC protein specifically in the 20,000 × g sediment (lane 5), indicating that the protein was not cytosolic. The protein was easily solubilized by a mild detergent (lane 8), suggesting that it may be associated with membranes or membrane-bounded organelles. Finally, immunofluorescent microscopy revealed dotted signals for ispC (fig. 9*B*), and these signals were not associated with mitochondria (fig. 9*C*) or DNA (fig. 9*D*). Cells typically had multiple fluorescent spots that were frequently located near mitochondria (fig. 9*E*). Staining for extranuclear DNA overlapped with mitochondrial fluorescence (fig. 9*F*) but not with ispC fluorescence (fig. 9*G*).

Discussion

Plastids in *P. marinus*

The presence of 6 MEP pathway genes (fig. 1), together with the lack of any MVA pathway genes, suggests that the MEP pathway is responsible for de novo isoprenoid synthesis in *P. marinus*. A little possibility cannot be ruled out that the MEP pathway is not functional because we have been unable to find an *ispD* ortholog, but it does not impact on our logic for proving the existence of plastids in *P. marinus* (see below). Of course, activity of the MEP pathway still requires characterization in order to further discuss plastid function; however, this is beyond the scope of the present study.

The *P. marinus* genes reported here are very likely relevant to plastids because the MEP pathway is specific to PBE, all PBEs have obtained the genes from essentially the same source (table 1), and all MEP pathway genes of *P. marinus* consistently group with them (figs. 2–7). Furthermore, the fact that all these genes have the bipartite targeting sequence (figs. 1 and 8), plus the fact that the predicted targeting sequences are cleaved (fig. 9*A*, lane 2), supports our idea that these enzymes traffic using machinery homologous to those of secondary PBEs. Finally, a subcellular fractionation experiment indicated that ispC is not cytosolic and is associated with membranes or organelles (fig. 9*A*, lanes 5 and 8), and immunofluorescent microscopy showed punctate localization of ispC near mitochondria (fig. 9*E*). Generally said, if a group of proteins accumulates at a subcellular compartment by means of machinery reasonably homologous to that of plastids, that compartment should be identified as a plastid. Although recent studies have shown the evidence for *P. marinus* plastid (Stelter et al. 2007; Teles-Grilo et al. 2007), no direct evidence that completely fulfills this criterion has been presented. To our knowledge, we are the first to use proper evidence in order to demonstrate that *P. marinus* harbors secondary plastids.

We revealed the existence of *P. marinus* plastids by detecting ispC using immunofluorescent microscopy. However, our SWIT analysis showed that ispF and PmSOD2 had similar but slightly different bipartite presequences (figs. 1 and 8). Although PmSOD2 has also shown punctate localization (Schott and Vasta 2003), it remains to be elucidated whether ispC and PmSOD2 are colocalized. Another point to be examined is that the ispC spots do not

overwrap with DNA signals (fig. 9*G*). Given that staining of mitochondrial DNA is definitive (fig. 9*F*), the putative plastids seem to contain very low quantities of DNA or may even lack DNA. Our preliminary search of the TIGR genome database suggests that *P. marinus* has genes for mitochondrial DNA and RNA polymerases, elongation factors, and ribosomal proteins but seemingly lacks those for plastid counterparts (data not shown). There are no examples in the literature of DNA-lacking plastids; however, we know of many independent reports that show modified or degenerated mitochondria that lack DNA (Hackstein et al. 2006). It is thus worth considering the possibility of DNA-lacking plastids in *P. marinus*, although this remains to be confirmed experimentally.

We have shown the presence of secondary plastids in *P. marinus* by immunofluorescent microscopy; however, no corresponding structure has been found in EM specimens sampled from the same culture (Kuroiwa H, unpublished data). Upon conducting a literature review, we found that 3 candidate ultrastructures have been observed in allied organisms. One is a "coiled membrane system" near the mitochondria that was found in the oldest observations of *P. marinus* zoosporulation (Perkins and Menzel 1967). Although this structure has been considered a morphological variant of the mitochondria, it could also be interpreted as a multimembrane-bounded plastid resembling the apicoplast of the malarial parasite *Plasmodium falciparum* (Hopkins et al. 1999). Another candidate structure is the "enigmatic body" found in a related organism, *Rastrimonas subtilis* (Brugerolle 2002, 2003), which is limited by 2 or more membranes and is akin to the apicoplast of *Toxoplasma gondii* in spherical appearance and juxtanuclear localization (Matsuzaki et al. 2001; Köhler 2005); however, the assumed relationship between *R. subtilis* and *Perkinsus* spp. is based only on morphology and is currently unsupported by molecular information. Finally, a putative plastid bounded by 4 membranes was recently reported in *P. olseni* (=*P. atlanticus*) (Teles-Grilo et al. 2007). If this is the plastid to which the MEP pathway enzymes target, connection between the TP with a transmembrane helix and a plastid bounded by 3 membranes should be reconsidered. It is interesting that all 3 candidate structures have been observed in the respective organisms' flagellated stage and that no relevant structures have been reported at the EM level from nonflagellated cultures. Our results indicate that the nonflagellated cultures contain plastids (fig. 9*B*). It is possible that the plastid is in a degenerated form and is therefore overlooked in the nonflagellated stages at the EM level and develops during the course of differentiation into the flagellated stages. Note that ultrastructure alone (e.g., number of membranes) is inadequate to identify plastids (Köhler 2006); immunological labeling of the ultrastructure is required for confirmation, for which our affinity-purified antibody to ispC would be useful.

That the putative *P. marinus* plastid and the peridinine plastids share a common origin was suggested by the phylogenetic affinity between some MEP pathway genes and those of the peridinine dinoflagellates and the predicted features of the *P. marinus* TPs. The *P. marinus* TPs predict that the putative plastid is bounded by 3 membranes because TP with transmembrane helix seems to correspond to plastids with 3 bounding membranes, such as those found in dinoflagellates and euglenoids (Patron et al. 2005). Given that *Perkinsus* spp. are located basally to dinoflagellates (Cavalier-Smith and Chao 2004; Leander and Keeling 2004), it is reasonable to suppose that a common ancestor harbored a plastid that diverged to form the *P. marinus* and peridinine plastids. *Perkinsus marinus* has TPs that are reminiscent of those found in peridinine dinoflagellates (fig. 1), although unusual TPs have been found in dinoflagellates containing haptophyte-derived plastids (Patron et al. 2006); thus, the result supports the hypothesis that haptophyte-derived plastids are a derived feature (Yoon et al. 2005). Study of the MEP pathway genes in other nonphotosynthetic taxa of Dinozoa, such as *Oxyrrhis*, *Syndinium*, and *Noctiluca*, may reveal the presence of cryptic plastids. On the other hand, the *Perkinsus* MEP pathway genes failed to show a relationship with apicomplexan orthologs (data not shown) possibly because the apicomplexan OTUs were a strong source of a long-branch attraction artifact. The relationship between the putative plastid of *P. marinus* and the apicoplast is thus still open question. Because the nonphotosynthetic free-living flagellates, *Colpodella* spp., are phylogenetically basal to the apicomplexans (Kuvardina et al. 2002; Cavalier-Smith and Chao 2004; Skovgaard et al. 2005), investigating whether *Colpodella* contains plastids would be interesting. The putative plastid in *P. marinus* will be a key to verifying the chromalveolate hypothesis and will partially rebut its critics (Bodył 2005).

Implications for Plastid Evolution

Our phylogenetic analyses showed that the MEP pathway of PBEs has an apparently mosaic origin in Cyanobacteria, Proteobacteria, and Chlamydia (table 1). Although an earlier study with limited sampling gave similar results for 5 genes (dxs to ispF) (Lange et al. 2000), the present results reinforce the evolutionary origins by using a wide range of bacteria. We also showed that the mosaic pattern was essentially the same among PBEs, including *P. marinus*, as is often the case with other plastid-related mosaic pathways, such as the Calvin cycle, heme biosynthesis, and the shikimate pathway (Matsuzaki et al. 2004; Obornik and Green 2005; Richards et al. 2006). Thus, we assume that the mosaic pattern was established before radiation of a wide variety of plastids, again supporting a single origin for plastids (Bhattacharya et al. 2004; Matsuzaki et al. 2004). It is natural that the cyanobacterial genes would be introduced during the primary endosymbiotic event, but the contribution of chlamydial genes seems rather peculiar. The apparent affinity could be interpreted as an artifact of interbacterial gene replacement (Lange et al. 2000; Rujan and Martin 2001); however, we consider that the observed mosaic pattern reflects an actual contribution by Chlamydia, because Chlamydia-related higher plant genes are biased toward plastid functions (Brinkman et al. 2002), and the bias is difficult to explain without assuming a connection between Chlamydia and plastids.

The ispG alignment (supplementary fig. S2, Supplementary Material online) and phylogenetic tree (fig. 6) show that the origin of the red algal orthologs clearly differed from that of orthologs from other PBEs. This seems

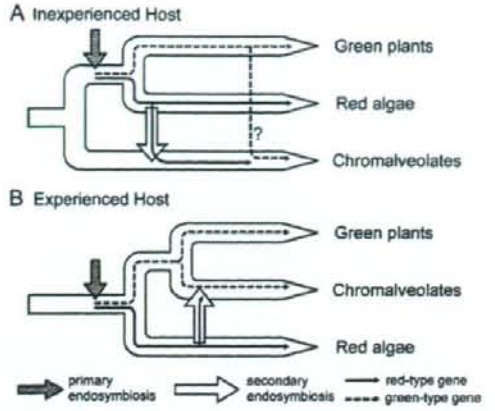

FIG. 10.—Explanation of the phylogenetic affinity to green plants in the cyanobacterial genes from chromalveolates, in 2 alternative phylogenetic trees of the host eukaryotes. (*A*) The inexperienced host model. If the ancestral chromalveolate host was inexperienced with primary plastids, red-type genes (solid arrows) must have been introduced and used in the chromalveolates at the secondary endosymbiotic event (unfilled arrow). Then, the green-type genes (broken arrows) may have been introduced via an unknown lateral gene transfer (LGT) event (indicated by "?") and replaced the red-type genes. (*B*) The experienced host model. Assuming that the ancestral host organism was experienced with primary plastids, 2 options exist for the secondary endosymbiotic event: retaining the green-type genes inherited from the ancestor or accepting the red-type genes transferred from the symbiont. In this case, the discrepancy can be explained without any further LGT event.

unusual, but other genes also show a similar difference between red algae and other PBEs, for example, enoyl acyl carrier protein reductase (Matsuzaki M, unpublished data) and plastid ferrochelatase (Obornik and Green 2005). This discrepancy in the phylogenetic positions of genes in red algae and the chromalveolates can be explained by the evolutionary histories of the symbiotic hosts (fig. 10). Two competing inferences exist for PBE phylogeny: the chromalveolates are independent of primary PBEs and are inexperienced with primary plastids (Rodríguez-Ezpeleta et al. 2005) (fig. 10*A*) and the chromalveolates originate from an in-group of primary PBEs and are experienced with primary plastids (Nozaki et al. 2003, 2007) (fig. 10*B*). Because it is widely accepted that the plastid progenitor in the chromalveolates is a kind of, or belongs to a sister group of, ancestral red algae (Fast et al. 2001; Yoon et al. 2002, 2005), the former topology predicts that red algae and the chromalveolates contain genes of the same cyanobacterial origin and requires extra loss, gain, or transfer events to explain the observed differences (fig. 10*A* shows a transfer event from the green plant lineage, which is the simplest). For the latter topology, the chromalveolates have 2 possible sources for plastid genes, the host ancestor and the symbiont. In this scenario, genes related to those of green plants can be inherited as constituents of the host genome and can be retained and used after the secondary endosymbiotic event. We prefer the latter model (fig. 10*B*) because it does not require additional transfer events other than the 2 widely accepted endosymbiotic events. In addition, this scenario can explain the frequently observed incoherence of the phylogenetic affinity of diatom genes, for example, the MEP pathway (figs. 2–7), the shikimate pathway (Richards et al. 2006), and the heme biosynthesis pathway (Obornik and Green 2005), in which the diatom ortholog for each gene has phylogenetic affinities to either green plants or red algae. Genes with an affinity to green plants and red algae could be derived from the host eukaryote and the plastid progenitor at the secondary symbiotic event, respectively. Furthermore, this scenario implies that the host eukaryote of the secondary endosymbiotic event that forms the chromalveolate ancestor must have retained the primary plastid originating from the ancient primary endosymbiosis because the MEP pathway seems to be specific to PBEs; then, it was replaced with the secondary plastid obtained from the engulfed red alga.

Conclusion

The existence of the plastid and its affinity to those of dinoflagellates, as suggested in the present study, greatly changes our view of *P. marinus*. It was first described as a pathogenic protist, then subsequently reclassified as a fungal or sporozoan species, and has recently been treated as an alveolate flagellate (Villalba et al. 2004; Adl et al. 2005); however, *P. marinus* is a cryptic alga in terms of plastid existence. Our identification of a *Perkinsus* spp. plastid will make this algal organism key in discussions of plastid evolution. Furthermore, just as discovery of the apicoplast has revolutionized malaria chemotherapy, the algal nature of *Perkinsus* spp. may permit novel approaches for controlling perkinsosis in fisheries.

Supplementary Material

Supplementary tables S1–S3 and figures S1–S3 are available at *Molecular Biology and Evolution* online (http://www.mbe.oxfordjournals.org/).

Acknowledgments

Preliminary sequence data for *P. marinus* were obtained from The Institute for Genomic Research via their Web site at http://www.tigr.org/. Sequencing of the *P. marinus* genome was accomplished with support from the US National Science Foundation. The genome sequence data for *Galdieria sulphuraria* were obtained from the Michigan State University Galdieria Database (http://genomics.msu.edu/galdieria/). The genome sequence data for *Chlamydomonas reinhardtii*, *Ostreococcus lucimarinus*, *Phaeodactylum tricornutum*, and *Thalassiosira pseudonana* were obtained from the US Department of Energy Joint Genome Institute (http://www.jgi.doe.gov/) and are provided for use in this publication only. The authors thank Dr Shin-ichiro Maruyama and Dr Takashi Nakada (the University of Tokyo) for helpful discussions and comments on figure presentation and Dr Shigeharu Sato (National Institute for Medical Research, UK) for providing valuable information on related topics. This study was supported by Grants-in-Aid

for Creative Scientific Research (16GS0304 to H.N. and 18GS0314 to K.K.), for Scientific Research (17370087 to H.N. and 18073004 for K.K.), and for the Japan Society for the Promotion of Science (JSPS) Fellows (17-10695 to M.M.) from the JSPS and the Ministry of Education, Culture, Sports, Science, and Technology (MEXT); by a matching fund subsidy for "Academic Frontier" Projects (to T.K.) from MEXT; and by the Program for the Promotion of Basic Research Activities for Innovative Biosciences (to T.K.). M.M. is a Research Fellow of the JSPS.

Literature Cited

Adl SM, Simpson AGB, Farmer MA, et al. (28 co-authors). 2005. The new higher level classification of eukaryotes with emphasis on the taxonomy of protists. J Eukaryot Microbiol. 52:399–451.

Armougom F, Moretti S, Poirot O, Audic S, Dumas P, Schaeli B, Keduas V, Notredame C. 2006. Expresso: automatic incorporation of structural information in multiple sequence alignments using 3D-Coffee. Nucleic Acids Res. 34:W604–W608.

Bendtsen JD, Nielsen H, von Heijne G, Brunak S. 2004. Improved prediction of signal peptides: signalP 3.0. J Mol Biol. 340:783–795.

Bhattacharya D, Yoon HS, Hackett JD. 2004. Photosynthetic eukaryotes unite: endosymbiosis connects the dots. Bioessays. 26:50–60.

Bodył A. 2005. Do plastid-related characters support the chromalveolate hypothesis? J Phycol. 41:712–719.

Brinkman FSL, Blanchard JL, Cherkasov A, et al. (14 co-authors). 2002. Evidence that plant-like genes in Chlamydia species reflect an ancestral relationship between Chlamydiaceae, cyanobacteria, and the chloroplast. Genome Res. 12:1159–1167.

Brugerolle G. 2002. *Cryptophagus subtilis*: a new parasite of cryptophytes affiliated with the Perkinsozoa lineage. Eur J Protistol. 37:379–390.

Brugerolle G. 2003. Apicomplexan parasite *Cryptophagus* renamed *Rastrimonas* gen. nov. Eur J Protistol. 39:101.

Cavalier-Smith T. 1999. Principles of protein and lipid targeting in secondary symbiogenesis: euglenoid, dinoflagellate, and sporozoan plastid origins and the eukaryote family tree. J Eukaryot Microbiol. 46:347–366.

Cavalier-Smith T, Chao EE. 2004. Protalveolate phylogeny and systematics and the origins of Sporozoa and dinoflagellates (phylum Myzozoa nom. nov.). Eur J Protistol. 40:185–212.

Derelle E, Ferraz C, Rombauts S, et al. (26 co-authors). 2006. Genome analysis of the smallest free-living eukaryote *Ostreococcus tauri* unveils many unique features. Proc Natl Acad Sci USA. 103:11647–11652.

Edgar RC. 2004. MUSCLE: multiple sequence alignment with high accuracy and high throughput. Nucleic Acids Res. 32:1792–1797.

Emanuelsson O, Nielsen H, Brunak S, von Heijne G. 2000. Predicting subcellular localization of proteins based on their N-terminal amino acid sequence. J Mol Biol. 300:1005–1016.

Fast NM, Kissinger JC, Roos DS, Keeling PJ. 2001. Nuclear-encoded, plastid-targeted genes suggest a single common origin for apicomplexan and dinoflagellate plastids. Mol Biol Evol. 18:418–426.

Gardner MJ, Bishop R, Shah T, et al. (44 co-authors). 2005. Genome sequence of *Theileria parva*, a bovine pathogen that transforms lymphocytes. Science. 309:134–137.

Gardner MJ, Hall N, Fung E, et al. (45 co-authors). 2002. Genome sequence of the human malaria parasite *Plasmodium falciparum*. Nature. 419:498–511.

Goto N, Nakao MC, Kawashima S. 2003. BioRuby: open-source bioinformatics library. Genome Inform. 14:629–630.

Guindon S, Gascuel O. 2003. A simple, fast, and accurate algorithm to estimate large phylogenies by maximum likelihood. Syst Biol. 52:696–704.

Hackstein JHP, Tjaden J, Huynen M. 2006. Mitochondria, hydrogenosomes and mitosomes: products of evolutionary tinkering! Curr Genet. 50:225–245.

Hirokawa T, Boon-Chieng S, Mitaku S. 1998. SOSUI: classification and secondary structure prediction system for membrane proteins. Bioinformatics. 14:378–379.

Hopkins J, Fowler R, Krishna S, Wilson I, Mitchell G, Bannister L. 1999. The plastid in *Plasmodium falciparum* asexual blood stages: a three-dimensional ultrastructural analysis. Protist. 150:283–295.

Köhler S. 2005. Multi-membrane-bound structures of Apicomplexa: I. the architecture of the *Toxoplasma gondii* apicoplast. Parasitol Res. 96:258–272.

Köhler S. 2006. Multi-membrane-bound structures of Apicomplexa: II. the ovoid mitochondrial cytoplasmic (OMC) complex of *Toxoplasma gondii* tachyzoites. Parasitol Res. 98: 355–369.

Kuvardina ON, Leander BS, Aleshin VV, Myl'nikov AP, Keeling PJ, Simdyanov TG. 2002. The phylogeny of colpodellids (Alveolata) using small subunit rRNA gene sequences suggests they are the free-living sister group to apicomplexans. J Eukaryot Microbiol. 49:498–504.

Lange BM, Rujan T, Martin W, Croteau R. 2000. Isoprenoid biosynthesis: the evolution of two ancient and distinct pathways across genomes. Proc Natl Acad Sci USA. 97:13172–13177.

Leander BS, Keeling PJ. 2004. Early evolutionary history of dinoflagellates and apicomplexans (Alveolata) as inferred from hsp90 and actin phylogenies. J Phycol. 40:341–350.

Matsuzaki M, Kikuchi T, Kita K, Kojima S, Kuroiwa T. 2001. Large amounts of apicoplast nucleoid DNA and its segregation in *Toxoplasma gondii*. Protoplasma. 218:180–191.

Matsuzaki M, Misumi O, Shin-i T, et al. (42 co-authors). 2004. Genome sequence of the ultrasmall unicellular red alga *Cyanidioschyzon merolae* 10D. Nature. 428:653–657.

Nielsen H, Engelbrecht J, Brunak S, von Heijne G. 1997. Identification of prokaryotic and eukaryotic signal peptides and prediction of their cleavage sites. Protein Eng. 10:1–6.

Nielsen H, Krogh A. 1998. Prediction of signal peptides and signal anchors by a hidden Markov model. Proc Int Conf Intell Syst Mol Biol. 6:122–130.

Not F, Valentin K, Romari K, Lovejoy C, Massana R, Töbe K, Vaulot D, Medlin LK. 2007. Picobiliphytes: a marine picoplanktonic algal group with unknown affinities to other eukaryotes. Science. 315:253–255.

Nozaki H, Iseki M, Hasegawa M, Misawa K, Nakada T, Sasaki N, Watanabe M. 2007. Phylogeny of primary photosynthetic eukaryotes as deduced from slowly evolving nuclear genes. Mol Biol Evol. 24:1592–1595.

Nozaki H, Matsuzaki M, Takahara M, Misumi O, Kuroiwa H, Hasegawa M, Shin-i T, Kohara Y, Ogasawara N, Kuroiwa T. 2003. The phylogenetic position of red algae revealed by multiple nuclear genes from mitochondria-containing eukaryotes and an alternative hypothesis on the origin of plastids. J Mol Evol. 56:485–497.

Obornik M, Green BR. 2005. Mosaic origin of the heme biosynthesis pathway in photosynthetic eukaryotes. Mol Biol Evol. 22:2343–2353.